

# Chapter 5

## Design, analysis and validation of MPPT for non-uniform weather conditions

*This chapter initially explains the partial shading phenomenon and its adverse effects on the power output of PV array along with a critical overview about the advanced MPPTs present in literature for non-uniform conditions. After that, partial shading has been studied extensively using comprehensive models developed in Matlab/Simulink and some critical observations are noted. Based on these observations, a new MPPT is designed specifically for partial shading. A new Proportional-controller based pulse width modulation of duty cycle is developed, which works in association with the proposed MPPT. Furthermore, a fine-tuning in the proposed technique and possible merger of this technique with the MPPT of uniform condition (designed in Ch. 4) is also presented. Numerous simulation and experimental studies are conducted to validate the effectiveness of the proposed technique compared to the past-proposed MPPTs.*

### **5.1 Partial shading phenomenon and literature survey of MPPTs**

The maximum power point tracking (MPPT) method is usually an essential part of a PV system because of the nonlinear characteristics of PV array. Under uniform atmospheric conditions, the PV array exhibits a single maximum power point (MPP) which can be tracked using conventional MPPT techniques [69]. Under partial shading conditions, the situation becomes more complicated as PV array executes multiple local maxima (LMs) [34,70-72], one of them is a global maximum (GM). Partial shading is a phenomenon when some modules within a PV array receive different irradiance levels due to dust, cloudy weather or from the shadows of nearby

buildings, trees, mountains etc. Indeed, partial shading is practically unavoidable in building integrated PV systems. Unfortunately, conventional MPPT methods are not capable enough to handle partial shading conditions. According to [21,73], the power losses due to the MPPT algorithm convergence to a local maximum (LM) instead of the GM may be up to 70%. Therefore, it is necessary to develop modified MPPT schemes that can search the GM from all the available LMs.

Figure 5.1(a) shows a more practical arrangement of a PV array, in which two types of diodes (bypass and blocking) are connected. During partial shading, several series PV modules are less illuminated and behave as a load instead of a generator [42-43,78]. This condition reduces the total power generation and may cause hot-spot problem [44]. In order to protect modules from the hot-spot problem, one or more bypass diodes are connected in parallel with a group of cells in each PV module [46]. However, blocking diodes are connected at the end of each PV string to protect the array from being affected by the current imbalance between the strings.

Figure 5.1(a) shows that the PV array receives a uniform irradiance, the bypass diodes of every string are reverse biased. Consequently, the PV current flows through the series PV modules and the resulting P-V curve exhibits a single MPP. However,

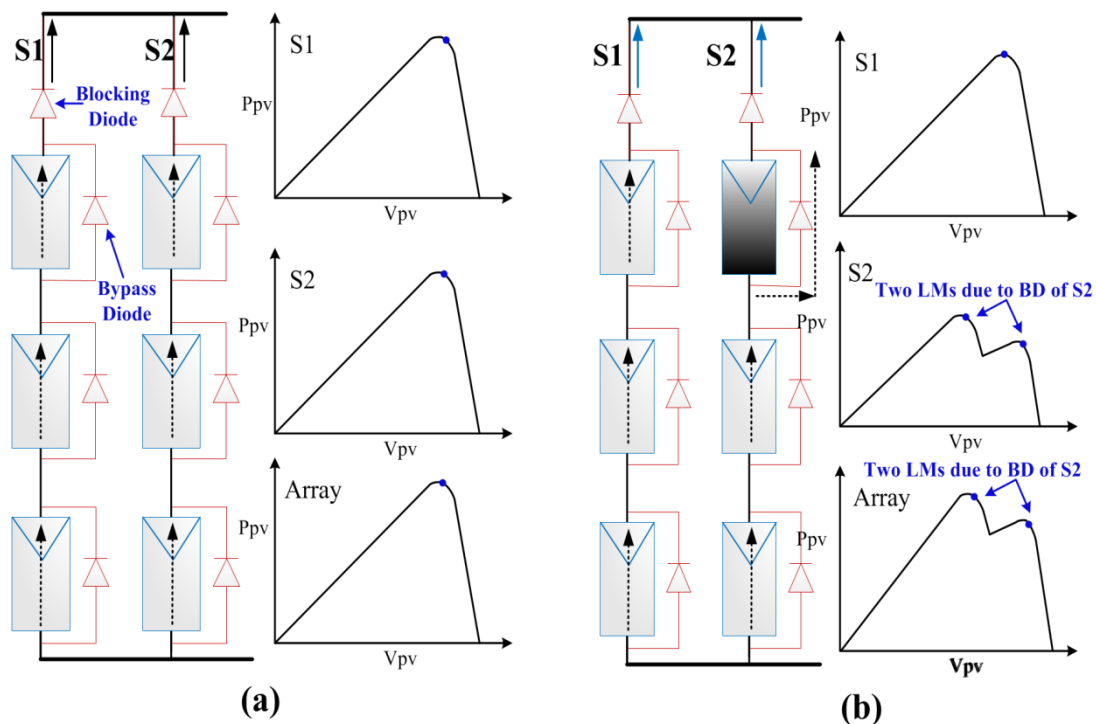


**Figure 5.1** – Protection diodes role in a PV array

during partial shading conditions as shown in Fig. 5.1(b), string S1 receives the uniform irradiance level, but the shaded module of string S2 receives a reduced solar irradiance. The difference in voltage between the two distinct irradiated modules of S2 turns on the bypass diode of the shaded module [32,34,70-72]. As a result, the resulting P-V curve for S2 is characterized by two LMs. It can be confirmed that during partial shading, the activation of bypass diodes transforms the P-V curve into more complicated curve — characterized by multiple LMs [32,34,41,70-72].

To date, various MPPT techniques have been designed for partial shading conditions and some of them have surveyed by [20,27]. In [73], a load line based MPPT is proposed. This MPPT has a drawback that its accuracy can degrade with aging of electrical components. A technique based on slope of power curve has been proposed in [16]. This MPPT is accurate in locating the GM, but has low convergence speed, whereas the power increment based MPPT presented in [21] has fast convergence speed but requires two PWM units. The MPPT technique presented in [74] requires less voltage perturbations to search the GM. A drawback of this technique is that it always scans the complete P-V curve under any kind of partial shading pattern.

On the other hand, many researchers have utilized advanced control methods to deal with partial shading conditions. In [75], a fuzzy logic controller based MPPT technique is presented whose controller parameters are optimized through a Hopfield neural network. Although this technique is accurate in detecting the GM vicinity, but the optimization process of this technique is not simple. To tackle partially shaded PV arrays, evolutionary algorithm based MPPTs have been proposed by many researchers such as differential evolution [76], particle swarm optimization [41] and ant colony optimization [77], which are efficient to search the GM. However, a common drawback of these methods is that they exhibit significant algorithmic complexity, which increases the implementation cost of the PV control systems.

In view of these drawbacks, this chapter presents a new technique (BD-MPPT) which is simple, yet more effective as compared to the past-proposed methods. Initially, the effects of partial shading on PV array are studied by using two comprehensive PV simulation models [32,34]. From this study, some observations

regarding the working mechanism of bypass diodes are noticed. These observations play a vital role in the designing of the proposed technique. BD-MPPT has three stages and each stage is designed with simple control schemes. The main idea of the proposed MPPT can be summarized in two points: 1) Not to scan the complete P-V curve needlessly by employing the new voltage limit ( $V_{LIM}$ ) mechanism and 2) Intelligent calibration of voltage steps such that the GM tracking process is accomplished with less voltage perturbations. The proposed technique is implemented in Matlab/Simulink and its performance is tested under various kinds of partial shading conditions.

After designing the proposed BD-MPPT, the technique is further modified to achieve the followings: 1) the technique can also expertly deal with uniform conditions and possibly, can be integrated to MPPT designed for uniform condition in Ch. 4 and 2) the tracking ability of algorithm to search GM is enhanced. To assist these techniques, a D-modulation control scheme based on  $k_p$  controller is also presented. To prove the performance of modified MPPT, several experimental tests are conducted. Furthermore, the advantage of modified MPPT over BD-MPPT is analyzed by applying MPPTs on 86.2 kW building integrated PV (BIPV).

## 5.2 Study of partial shading effects on PV array

In order to study the effects of partial shading on the PV array, Matlab/Simulink simulations have been carried out using two comprehensive PV

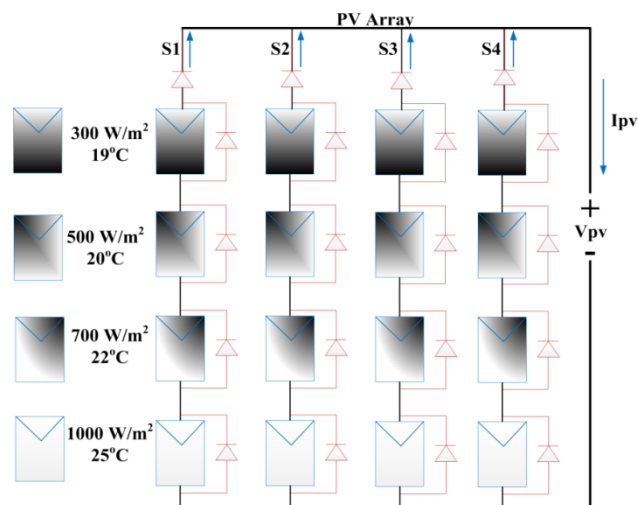


Figure 5.2 – PV array with shading pattern

model developed by [32,-34]. Fig. 5.2 shows the PV array with shading pattern, the behavior of which has been evaluated. PV array contains four strings while each string contains four modules, i.e. 4 x 4. Since short-circuit current of the PV array is proportional to irradiance while its open-circuit voltage depends upon temperature, different irradiance and temperature levels are used in the shading pattern as shown in Fig. 5.2. PV module ( $V_{oc} = 21.06$  V,  $I_{sc} = 3.8$  A at STC) has been used with the model-A [34]. While 60 W PV module ( $V_{oc} = 21.1$  V,  $I_{sc} = 3.8$  A,  $P_{mpp} = 60$  W,  $I_{MPP} = 3.5$  A and  $V_{mpp} = 17.15$  V at STC) has been used with the model-B [32].

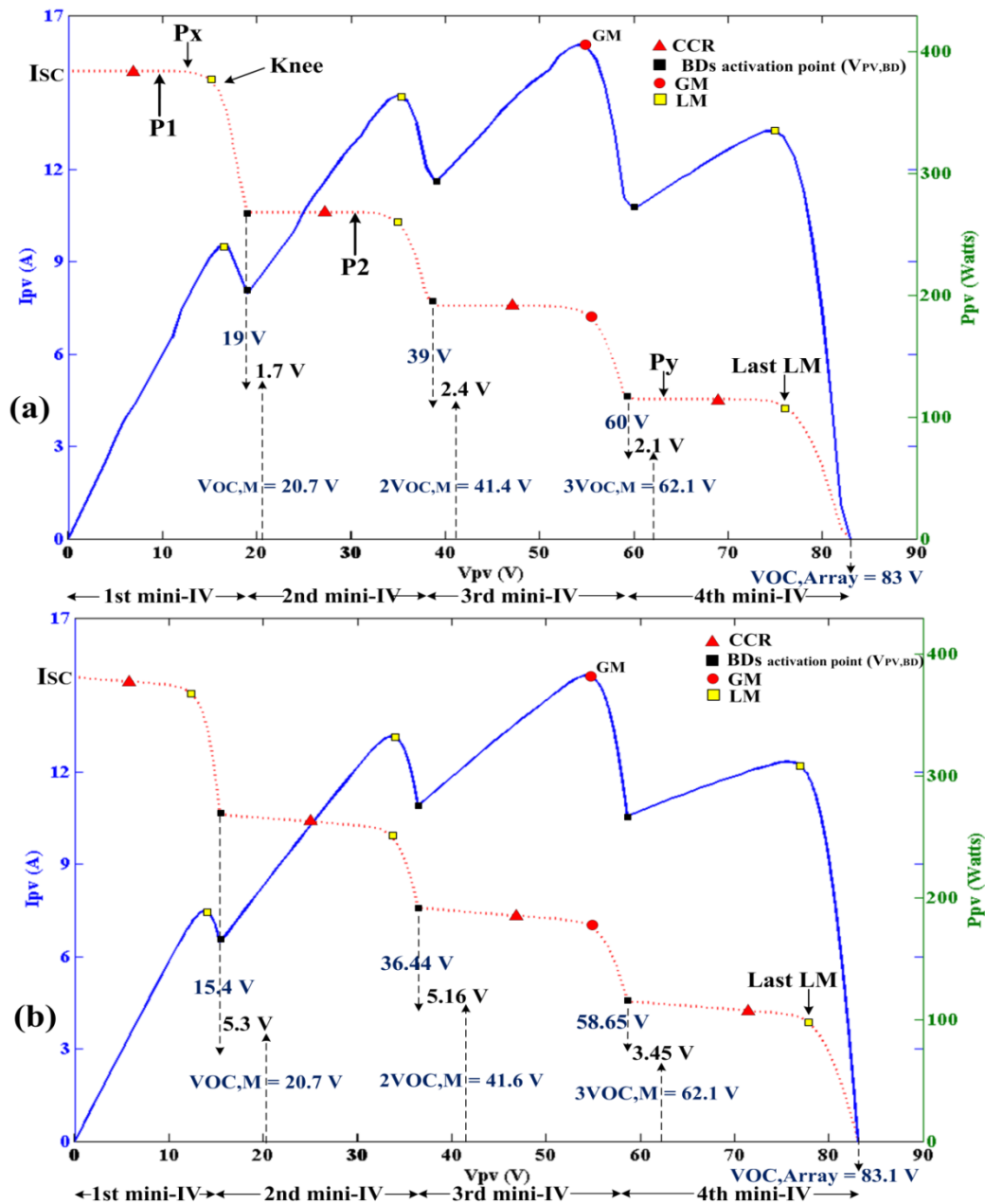


Figure 5.3 – I-V and P-V Curves of (a) PV model-A [34] and (b) PV model-B [32]

Figure 5.3(a) illustrates the current-voltage (I-V) and power-voltage (P-V) curves for the model-A [34] and Fig. 5.3(b) shows the I-V and P-V curves for the model-B [32]. P-V curves of both models contain four LMs. It can be evaluated from Fig. 5.3(a) that when bypass diodes of some shaded modules become forward biased at 19 V, this increases the current ( $I_{pv}$ ) of array at lower voltages. This transition in  $I_{pv}$  due to bypass diodes actually creates the LM. Like at 19 V,  $I_{pv}$  starts increasing and continues to increase up to point  $P_X$  (moving backwards). At  $P_X$ ,  $I_{pv}$  becomes constant and remains in the same state up to 0 V. In this way, a constant current region (CCR) between 0 -  $P_X$  and a knee (in which LM is present) near 19 V are occurred. Furthermore, if partial shading conditions are such that bypass diodes do not work at 19 V, then there will be no change in  $I_{pv}$  at this point. It means  $I_{pv}$  will remain constant from 19 V up to 0 V. Hence, only CCR will occur in this region and no LM.

Figure 5.3(a) shows that first LM has occurred between 0 - 19 V on I-V curve. For instance, if we sideline the rest of the I-V curve, then I-V curve between 0 - 19 V shows a behavior that is similar to the I-V curve of uniform irradiance. This mini-I-V curve contains a CCR and a knee (containing LM). Next LM is present between 19 - 39 V. This LM has also occurred due to the working of some bypass diodes at 39 V. Again a mini-I-V curve can be noticed between 19 - 39 V. Same is the case with the other two mini-I-V curves present between 39 - 60 V and 60 - 83 V. Similar phenomenon can be observed for the four mini-I-V curves (1st: 0 - 15.4 V, 2nd: 15.4 - 36.44 V, 3rd: 36.44 - 58.65 V and 4th: 58.65 - 83.1 V) shown in Fig. 5.3(b) i.e. a knee followed by a CCR.

Results presented in [16,41,74] demonstrated that the voltage ( $V_{PV,BD}$ ) values at which bypass diodes become activated, responsible for the mini-I-Vs, always occur at integral multiples of open-circuit voltage of the module ( $V_{OC,M}$ ) i.e.  $n \times V_{OC,M}$  where  $n$  is an integer.  $V_{OC,M}$  can be measured from the PV array, but it requires additional hardware arrangements. However,  $V_{OC,M}$  can be estimated with the help of open-circuit voltage of the array ( $V_{OC,Array}$ ) i.e.  $V_{OC,Array}/N_S$ , where  $N_S$  is the number of series connected modules in a given string. Figure 5.3(a) indicates that  $V_{OC,Array} = 83$  V and as  $N_S = 4$ , so  $V_{OC,M} = 20.7$  V. It can be seen that voltages  $V_{PV,BD}$  are around integral multiples of  $V_{OC,M}$ . The difference between 1st mini-I-V's  $V_{PV,BD}$  &  $V_{OC,M}$  is

1.7 V and between 2nd mini-I-V's  $V_{PV,BD}$  &  $2V_{OC,M}$  is 2.4V. However, the I-V curve of second model shows more offsets as shown in Fig. 5.3(b). Like the difference between 2nd mini-I-V's  $V_{PV,BD}$  &  $2V_{OC,M}$  is 5.16 V.

Figure 5.3(a) and Fig. 5.3(b) indicate that last LM always occur between second last  $V_{OC,M}$  ( $3V_{OC,M}$ ) and  $V_{OC,Array}$  ( $4V_{OC,M}$ ). It should be noted that bypass diodes are not responsible for this LM. In fact, one can call it as natural LM as it happened because  $I_{PV}$  of the PV array always becomes equal to zero at  $V_{OC,Array}$ , thus creating a knee and LM. Figure 5.3(a) shows that  $I_{PV}$  of point  $P_X$  is greater than  $I_{PV}$  of last LM. However,  $I_{PV}$  of point  $P_Y$  is almost same as that of  $I_{PV}$  of last LM. Therefore, if the P-V curve is viewed from left side, i.e. when  $I_{PV} = I_{SC}$  and voltage ( $V_{PV}$ ) of the array is zero, then at any point prior to the last LM, it can be confirmed that either  $I_{PV}$  of the present point will be reduced or remains at the same value at last LM.

Observations made from the study of partial shading effects using two PV models [A & B] are listed as follows:

- P-1) During partial shading conditions, mini-I-V curves on I-V curve are occurred due to bypass diodes of shaded modules.
- P-2) Activation points of bypass diodes occur approximately at  $V_{OC,M}$ ,  $2V_{OC,M}$ , ...,  $(N_S-1)V_{OC,M}$  with some offsets.
- P-3) Between every two consecutive  $V_{OC,M}$ , a CCR is always present.
- P-4) Last LM (natural LM) always occur between  $(N_S-1) \times V_{OC,M}$  and  $N_S \times V_{OC,M}$ , i.e.  $V_{OC,Array}$ .
- P-5) If the P-V curve is viewed from the left side, then at any point prior to last LM,  $I_{PV}$  of present point will be reduced or remains at the same value at last LM.

### 5.3 Design of the proposed BD-MPPT

The design of the proposed BD-MPPT revolves around five observations mentioned in Sec. 5.3. In this technique, the P-V curve is always scanned from the left side, i.e.  $V_{PV} = 0$  and  $I_{PV} = I_{SC}$ . Voltage parameters of the technique are designed in order to evaluate the PV array on CCRs, which are present between every consecutive

$V_{OC,M}$ . The proposed BD-MPPT works in three stages as shown in the flowchart in Fig. 5.4. Stage-1 is the configuration stage, stage-2 is the GM search mechanism and stage-3 contains the last two loops (R-MPP and S-Loop) of MPPT for uniform conditions, which are designed in the previous chapter.

### 5.3.1 Stage-1: Configuration stage

In this stage, the proposed BD-MPPT configures the voltage parameters using  $V_{OC,Array}$  information. It can be seen from the flowchart in Fig. 5.4 that technique measures  $V_{OC,Array}$  and then voltage step ( $\Delta V$ ), first voltage step ( $\Delta V_{1st}$ ) and voltage limit ( $V_{LIM}$ ) are configured according to the following relations:

$$\Delta V = V_{OC,M} \times \frac{1}{N_{BD,M}} = \frac{V_{OC,Array}}{N_S} \times \frac{1}{N_{BD,M}} \quad (5.1)$$

$$\Delta V_{1st} = \frac{\Delta V}{2} \quad (5.2)$$

$$V_{LIM} = \left( (N_S \times N_{BD,M}) - 1 \right) \times \Delta V + \Delta V_{1st} \quad (5.3)$$

Where,  $N_{BD,M}$  means the number of bypass diodes connected in parallel with a group of cells in a PV module.

**$\Delta V$ :** According to P-2 of Sec. 5.2, activation points of bypass diodes are at multiples of  $V_{OC,M}$ . Therefore,  $\Delta V$  of the technique is set at  $V_{OC,M}$ . However,  $N_{BD,M}$  is also taken into account in Eq. (5.1). It should be noted that whole discussion in Sec. 5.2 is based on PV modules with  $N_{BD,M} = 1$ . This means that each module contains a single bypass diode activation point. If  $N_{BD,M} = 3$ , then each module will contain three bypass diodes. Consequently, there will be three bypass diode activation points for each module. Hence,  $V_{OC,M}$  is divided by  $N_{BD,M}$  to adjust the step  $\Delta V$  accordingly.

**$\Delta V_{1st}$ :** Concerning the P-V curve presented in Fig. 5.3(a), where  $N_{BD,M} = 1$ ,  $\Delta V$  is estimated at 20.7 V. It means that with every step of  $\Delta V = 20.7$  V, the algorithm will reach almost that part of the P-V curve where activation of bypass diodes occurs, whereas the goal of the algorithm is to evaluate the PV array on CCRs. To achieve

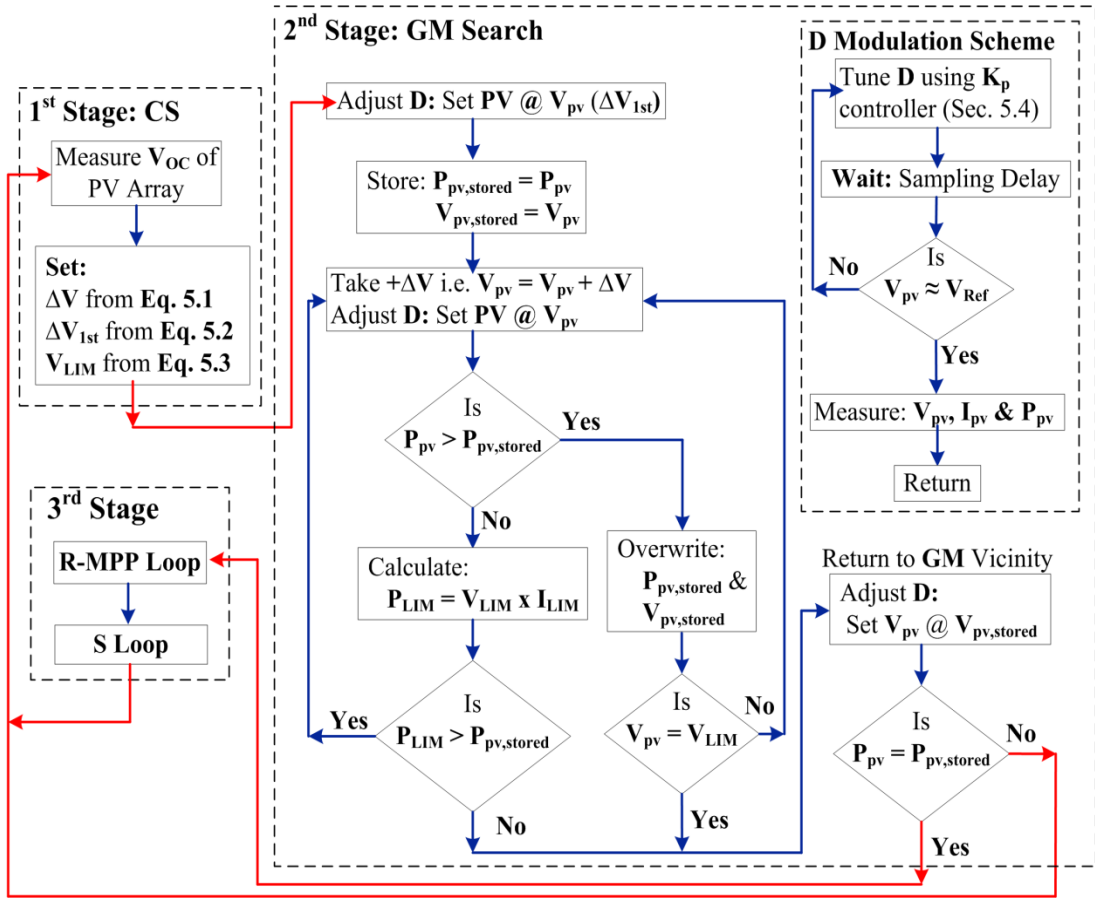


**Figure 5.4** – Working flowchart of the proposed BD-MPPT

this, the step  $\Delta V_{1st}$  is calibrated. BD-MPPT executes the first step of  $\Delta V_{1st}$ , which is half of  $\Delta V$  as given by Eq. (5.2). Afterwards, the technique will always utilize  $\Delta V$ . The first two steps of the technique are indicated on the I-V curve of Fig. 5.3(a). By taking  $\Delta V_{1st} = 10.35$  V, the algorithm reaches point P1 (CCR of the first mini-I-V) before  $V_{OC,M}$ . Next time, when  $\Delta V = 20.7$  V is taken, the technique will cross  $V_{OC,M}$  and reach on P2 (CCR of the second mini-I-V) before  $2V_{OC,M}$ . In this way, two goals are achieved: 1) Algorithm evaluates the PV array on CCRs which occurred between every consecutive  $V_{OC,M}$  according to P-3, and 2) As the algorithm is not moving exactly on  $V_{OC,M}$  values courtesy  $\Delta V_{1st}$ , the offset effect between bypass diodes activation point and  $V_{OC,M}$  is minimized.

**$V_{LIM}$** : The proposed method may scan the P-V curve up to  $V_{LIM}$  which is discussed in detail in stage-2. Since the last LM occurs between  $(N_S-1) \times V_{OC,M}$  and  $N_S \times V_{OC,M}$  ( $V_{OC,Array}$ ) according to P-4, the technique sets the  $V_{LIM}$  in this region. In

Eq. (5.3), consider  $N_{BD,M} = 1$ , and as  $\Delta V = V_{OC,M}$  so factor  $(N_S-1) \times \Delta V$  sets the  $V_{LIM}$  approximately at  $(N_S-1) \times V_{OC,M}$ . While, with the help of  $\Delta V_{1st}$ , the position of  $V_{LIM}$  is shifted in-between  $(N_S-1) \times V_{OC,M}$  and  $N_S \times V_{OC,M}$ .

### 5.3.2 Stage-2: GM search mechanism

The flowchart of GM search mechanism is shown in Fig. 5.4. It can be seen that after taking  $\Delta V_{1st}$ , the technique stores the power ( $P_{pv}$ ) and  $V_{pv}$  of the PV array. After first step, BD-MPPT always executes  $+\Delta V$ . At every  $+\Delta V$  step, if  $P_{pv}$  is greater than  $P_{pv,store}$ , then stored values ( $P_{pv,store}$  &  $V_{pv,store}$ ) will be overwritten with the new values. During these iterations, the algorithm checks that  $V_{LIM}$  is reached or not. Since  $V_{LIM}$  is checked when  $P_{pv}$  is greater than  $P_{pv,store}$ , then whenever  $V_{LIM}$  is reached, the algorithm realizes that GM is present at  $V_{LIM}$  i.e. last LM. Hence, the technique will move to stage-3 to reach GM precisely.

On every  $+\Delta V$  step, if  $P_{pv}$  is greater than  $P_{pv,store}$ , it is an ideal situation. Unfortunately, this is not the case everytime. Assume the partial shading case presented in Fig. 5.5, where the PV array contains  $N_S = 6$  and  $N_{BD,M} = 1$  while  $V_{OC,Array}$  is 126 V. Using (1), (2) and (3), the voltage parameters are configured as:  $\Delta V = 21$  V,  $\Delta V_{1st} = 10.5$  V and  $V_{LIM} = 115.5$  V. It can be seen that on the 3rd step (P3),  $P_{PV} = 437.1$  W is less than  $P_{PV,Stored} = 480$  W of P2. The algorithm should not stop the scanning here since P4 is the GM. One simple solution is to scan the complete P-V curve with  $\Delta V$  steps and then find out the maximum power value. However, this kind of solution has following shortcomings:

- 1) The convergence speed of the technique is compromised.
- 2) Since the power of every  $\Delta V$  step is stored, more storage memory is required.
- 3) After completing the scanning of the P-V curve, another embedded software algorithm is required which will look for the maximum power value from all the stored data, thus increasing the software complexity of the algorithm.

To avoid all these drawbacks,  $V_{LIM}$  mechanism is introduced. It should be noted that  $V_{LIM}$  is only invoked if, at any given point,  $P_{pv}$  is less than  $P_{pv,store}$  as shown in the flowchart in Fig. 5.4. The technique will estimate the power ( $P_{LIM}$ ) of

$V_{LIM}$  from the relation

$$\text{Real: } P_{LIM} = V_{LIM} \times I_{LIM} \quad (5.4)$$

$$\text{Estimation by BD-MPPT: } P_{LIM} = V_{LIM} \times I_{pv} \quad (5.5)$$

In Eq. (5.4),  $V_{LIM}$  is known from Eq. (5.3) but the current ( $I_{LIM}$ ) at  $V_{LIM}$  is not known. Scanning of the P-V curve is being executed from left side precisely to estimate  $I_{LIM}$ . It should be noted that the  $I_{pv}$  value of present point is available. Since BD-MPPT reaches the present point while scanning the P-V curve from left side therefore there will be only two possible scenarios according to P-5: Either  $I_{pv}$  of present point remains the same up to  $V_{LIM}$  or  $I_{pv}$  is reduced on  $V_{LIM}$ . Since one cannot predict how much the  $I_{pv}$  will reduce on  $V_{LIM}$ , the algorithm takes the latter option. The proposed technique assumes that  $I_{pv}$  of present point remains the same up to  $V_{LIM}$  and calculates  $P_{LIM}$  from Eq. (5.5). If the estimated  $P_{LIM}$  comes out to be greater than  $P_{pv,store}$ , the technique realizes that although at present point power is less. However, if the current remains at the same value, then there is a potential of more power at higher voltages. Hence, the technique will take  $+\Delta V$  without overwriting the values as

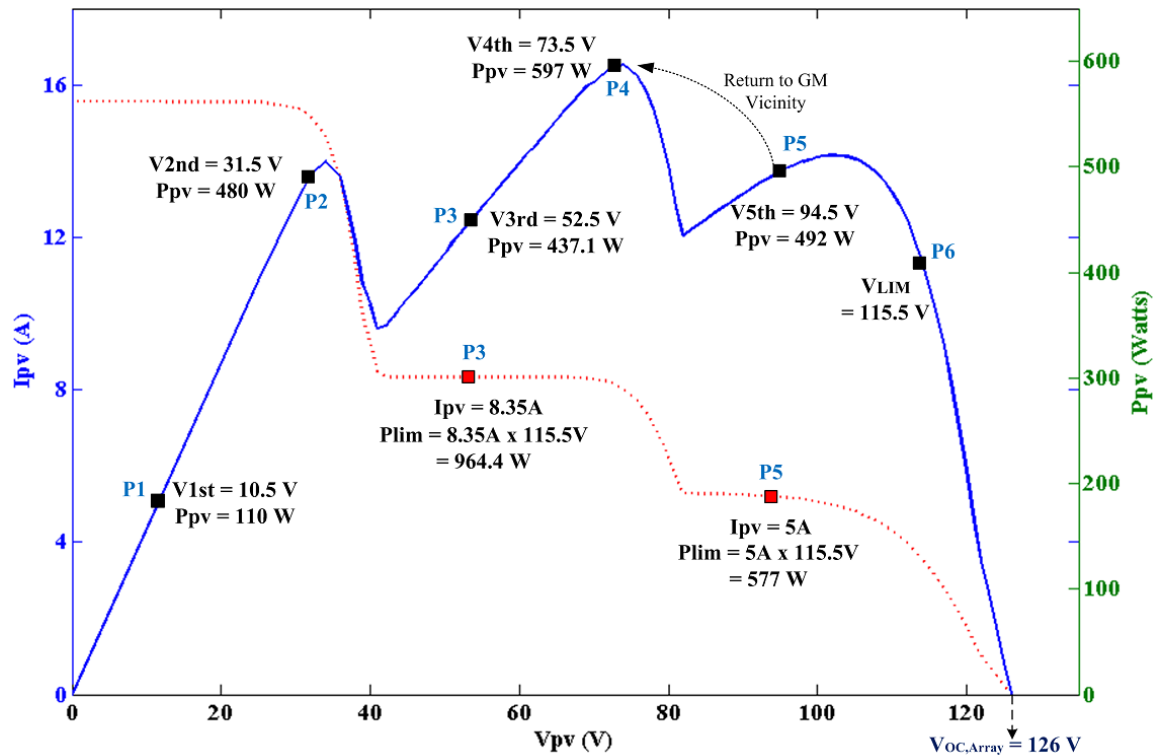


Figure 5.5 – Searching mechanism of global maximum

cleared from the flowchart shown in Fig. 5.4.

Figure 5.5 shows that at P3,  $P_{pv} = 437.1 \text{ W}$  is less than  $P_{pv,store} = 480 \text{ W}$  (P2), so the BD-MPPT activates the  $V_{LIM}$  mechanism. At this point, technique measures  $I_{pv} = 8.35 \text{ A}$  and calculates  $P_{LIM} = 964.4 \text{ W}$ . Because  $P_{LIM} = 964.4 \text{ W} > P_{pv,store} = 480 \text{ W}$  (P2), the technique takes  $+\Delta V$  without overwriting the values. At P4,  $P_{pv} = 597 \text{ W}$  is greater than  $P_{pv,store} = 480 \text{ W}$  (P2), so the technique overwrites the stored values and takes another  $+\Delta V$  step. At P5, since  $P_{pv} = 492 \text{ W} < P_{pv,store} = 597 \text{ W}$  (P4),  $V_{LIM}$  is again invoked. At this point,  $I_{pv} = 5 \text{ A}$  is measured by the technique which corresponds to  $P_{LIM} = 5 \text{ A} \times 115.5 \text{ V} = 577 \text{ W}$ . As  $P_{LIM} = 577 \text{ W}$  is also less than  $P_{pv,store} = 597 \text{ W}$  (P4), as a result, the algorithm will stop scanning process at P5. In this way, the algorithm skips the last point (P6) thus improving the convergence speed. At this point, the algorithm will return to the GM vicinity by setting the  $V_{pv}$  equals to  $V_{pv,store} = 73.5 \text{ V}$  as shown in the flowchart in Fig. 5.4. After returning to GM vicinity, the algorithm compares the two powers i.e.  $P_{pv}$  and  $P_{pv,store}$ . If the two powers are equal, the algorithm understands that partial shading conditions have not changed. Therefore, it will move to stage-3 otherwise to stage-1.

It should be noted that the maximum number of steps ( $Step_{Max}$ ) taken by BP-MPPT in order to detect the GM vicinity are always less than or equal to  $(N_S \times N_{BD,M}) + 1$  irrespective of any partial shading condition. However, under worst case:  $Step_{Max} = (N_S \times N_{BD,M}) + 1$ .

### 5.3.3 Stage-3: Real MPP and condition detection

After finding the vicinity of GM in stage-2, the algorithm will utilize the modified perturb and observe (P&O) method to reach GM precisely by taking small voltage perturbations. This modified P&O scheme is the same as that of the R-MPP loop of MPPT technique designed for uniform conditions in Ch. 4. After detecting the GM, the algorithm sticks to the GM and detects the weather conditions in the same manner as that of the S-loop of the MPPT of the previous chapter. Therefore, one can say that the stage-3 of the MPPT for partial shading contains the last two stages of MPPT for uniform condition i.e. Stage-3 = R-MPP  $\rightarrow$  Sloop as shown in flowchart in Fig. 5.4.

## 5.4 Pulse width modulation (PWM) of D of converter

It can be evaluated from flowchart in Fig. 5.4 that every time, when the algorithm updates the voltage steps, it needs to modulate the duty cycle (D) of the converter to bring the  $V_{pv}$  close to the desired/reference voltage. This leads to the conclusion that the MPPT should contain an efficient scheme that can regulate the  $V_{pv}$  of the array by pulse width modulation of D.

Using the digital processing devices of present-era, the complex algorithm (to estimate  $V_{Ref}$  value) can be computed merely in micro-seconds. But, while dealing with D-modulation scheme, the MPPT designer has to wait for some duration known as sampling delay/rate ( $S_{Rate}$ ) [56,67], after every change in PWM of D. The sampling rate, normally varies from 5 ms to 50 ms [56], is essential for the steady state operation of the PV system. Although estimation of reference point is equally important, but the time response ( $T_R$ ) of the MPPT is mainly determined by the effectiveness of the D-modulation scheme as indicated by relation:

$$T_R = T_P + N_s \times S_{Rate} \cong N_s \times S_{Rate} \quad (5.6)$$

Since the processing time ( $T_p$ ) of present-era digital devices is fast (in micro-seconds) and  $S_{Rate}$  is in milli-seconds,  $T_p$  can be neglected. Consequently, the  $T_R$  of MPPT depends upon that the number of samples ( $N_s$ ) required by the D-modulation mechanism to make  $V_{pv}$  close to  $V_{Ref}$ . It is natural that MPPT designers employed the services of conventional controllers (P/PI etc.) because of their low-cost implementation and maintenance [41]. However, due to the nonlinear characteristics of PV system, conventional controllers tend to lose their performance when employed in PV system [80]. This problem arises because the tuning criteria of controller gains are not properly discussed with respect to PV systems. Furthermore, D of the converter should always be computed within boundary limits i.e.  $0 < D < 1$  as already discussed in Ch. 3. It is possible that the improper tuning of controller gains may compute D out of boundary limits due to which the PV system may become unstable.

In view of these drawbacks, a modified PWM control scheme to compute D for PV systems is presented in this section, which mainly contains the P-controller. The contributions of this scheme are summarized as:

- The working principle of the proposed scheme is designed in such a manner that it eliminates the oscillations inherited by P-controller and its complexity remains low.
- The tuning criterion of  $k_p$  gain is properly formulated with respect to PV arrays under two kinds of loads i.e. resistive and battery. Hence, no hit and trial method or complex control procedures are required to tune the  $k_p$  gain. Furthermore, the relations indicate that  $k_p$  gain is adaptive for resistive load while it is static for battery load.
- Boundary limits of D ( $0 < D < 1$ ) of converter are properly addressed.
- Less sensory information required compared to past control schemes. Thus making it cost effective.

#### 5.4.1 D-modulation control schemes

The mechanism of proposed D-modulation scheme and other schemes are shown in Fig. 5.6. Figure 5.6(a) presents a simple D-modulation control scheme [51] for the boost converter. In this scheme, D is generated from the following relation:

$$D = 1 - \frac{V_{Ref}}{V_o} \quad (5.7)$$

Where,  $V_{Ref}$  is the reference voltage obtained using the MPPT algorithm and  $V_o$  is the output voltage of the converter. It is observed that the response of such controller is slow [16,81] when employing in PV systems. Therefore, this controller may struggle in fast varying weather conditions. To overcome this drawback, a new control scheme has been proposed by [16], which is shown in Fig. 5.6(b). This scheme introduces the P-controller ( $\Delta D$ ) in the Eq. (5.7) and can be mathematically expressed:

$$D = D^* - \Delta D \quad (5.8)$$

Where,  $D^* = 1 - (V_{Ref} / V_o)$  and  $\Delta D = k_p \times \text{error} = k_p \times (V_{Ref} - V_{pv})$ . This scheme works on the principle that the additional disturbance  $\Delta D$ , when subtracted from the actual duty cycle  $D^*$ , amplifies the disturbance towards MPP, and therefore, the MPP is attained quickly. However, this scheme has the following shortcomings: 1) Sensor may be required to measure  $V_o$ , 2) Tuning criteria of  $k_p$  is not discussed,

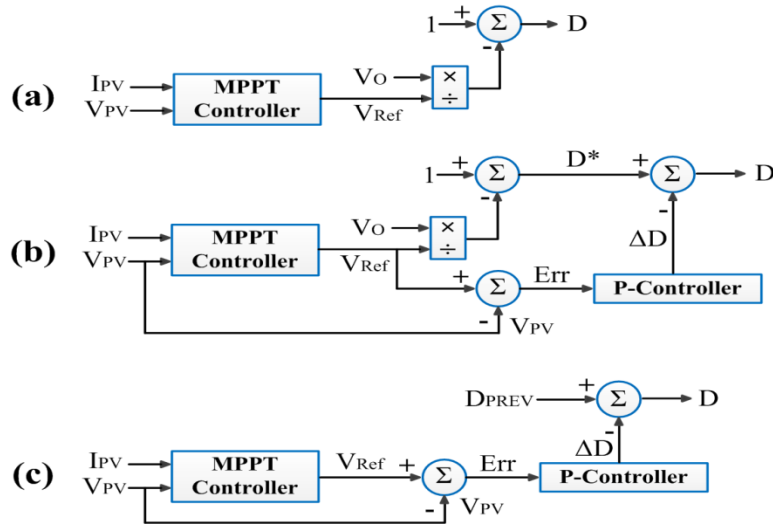


**Figure 5.6** – D-Modulation control schemes: a) Scheme [55], b) Scheme [16] and c) Proposed Scheme

3) Boundary limit criteria ( $0 < D < 1$ ) is not given, i.e. it is mathematically possible with Eq. (5.8) that  $D$  can go beyond these limits, and 4) In case, if the value of  $D^*$  is such that it sets the  $V_{pv}$  exactly on  $V_{Ref}$ , then  $\Delta D$  produces extra disturbance in  $D$ , which shifts  $V_{pv}$  away from  $V_{Ref}$ . To tackle all these drawbacks, a new D-modulation control scheme is proposed, which is shown in Fig. 5.6(c). This control scheme can be expressed in mathematical form as:

$$D = D_{prev} - \Delta D \quad (5.9)$$

Where,  $D_{prev}$  is the duty cycle of the previous iteration and  $\Delta D = k_p \times \text{error} = k_p \times (V_{Ref} - V_{pv})$ . Generally, a P-controller ( $k_p \times \text{error}$ ) operates with a steady-state error which results in oscillations around the reference. However, Eq. (5.9) explains that for the proposed scheme whenever error is equal to zero,  $D$  is always equal to  $D_{prev}$ , which implies that P-controller produces no effect as the proposed scheme has the information of history i.e.  $D_{prev}$ . In this way, the steady state oscillations inherited by P-controller doesn't exist in the proposed scheme. P-controller can only become active when there is some error. The principle involved in this scheme can be mathematically explained with the help of Fig. 5.7, where the relation between  $D$  and  $V_{pv}$  of the array is shown. As discussed in Ch. 2, to attain the high voltage values, the  $D$  will be reduced. Consider that MPPT algorithm sets the  $V_{Ref}$  equal to 36.4 V and

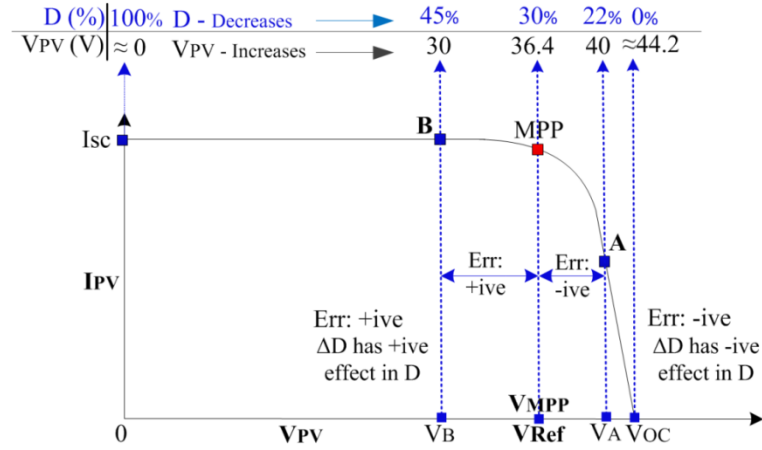


**Figure 5.7** – Duty cycle and  $V_{pv}$  relation of PV array

sends it to proposed D-modulation scheme, which can only be attained when the proposed scheme sets the D of converter at 0.3 (30%). Assuming that the proposed scheme sets the D at 0.22 (22%), as a result the PV array reaches point A. At this point, error is -ive as  $V_{pv}$  ( $= V_A$ ) is greater than  $V_{Ref}$ . Therefore, for the next D, Eq. (5.9) takes the form as:

$$D = D_{prev} - \Delta D = 0.22 + k_p \times error \quad (5.10)$$

It means that when error is -ive,  $\Delta D$  produces a +ive effect in D. This phenomenon can be seen from Fig. (5.7) that to move from A to MPP, D has to be increased. On the other hand, consider that the proposed scheme sets D at 0.45 (45%) as a result of which the PV array reaches point B. In this case, error is +ive as  $V_{pv}$  ( $= V_B$ ) is less than  $V_{Ref}$ , therefore Eq. (5.9) takes the form as:

$$D = D_{prev} - \Delta D = 0.45 - k_p \times error \quad (5.11)$$

Consequently when error is +ive,  $\Delta D$  produces a -ive effect in D, which is required in order to move from B to MPP.

### 5.4.2 Tuning of proposed D-modulation scheme

In this section, the relations are developed to set the  $k_p$  gain for both resistive and battery loads. The tuning criterion is discussed with respect to boost converter. However, same procedure can be applied for the other converters. Eq. (5.9) describes the working principle of proposed scheme can be re-written as:

$$D = D_{prev} - k_p \times error = D_{prev} - k_p(V_{Ref} - V_{pv}) \quad (5.12)$$

Under initial condition, i.e.  $t = 0$ , we can write

$$D = D_{t=0} - k_p(V_{Ref} - V_{pv,t=0}) \quad (5.13)$$

The above equation can be simplified further by considering that under initial condition, i.e.  $t = 0$ , PV array is operating with 100% duty cycle ( $D_{t=0} = 1$ ). This implies that PV array is under short-circuit condition, which can be realized from Fig. 5.7, therefore putting  $V_{pv,t} = 0$  in Eq. (5.13), we get

$$D = 1 - k_p \times V_{Ref} \quad (5.14)$$

Since the data at STC ( $1000 \text{ W/m}^2 - 25^\circ\text{C}$ ) of PV module can be obtained from Manufacturer's datasheet,  $V_{Ref}$  is set at voltage of MPP under STC condition, i.e.  $V_{mpp,STC}$ , which corresponds to  $D_{mpp,STC}$  i.e.  $D = D_{mpp,STC}$ . Putting these STC variables in Eq. (5.14) in order to calculate the  $k_{p,STC}$  as:

$$k_{p,STC} = \frac{1 - D_{STC}}{V_{mpp,STC}} \quad (5.15)$$

Although  $V_{mpp,STC}$  can be attained from Manufacturer's datasheet, but information regarding  $D_{STC}$  is not available. Another concern is that even if the value of  $D_{STC}$  is resolved, the  $k_{p,STC}$  gain is valid for all types of weather conditions as it is tuned according to STC data.

#### 5.4.2.1 Tuning of $k_p$ for resistive load

We know that while dealing with resistive load, the current ( $I_{pv}$ ) of array will produce a major impact. To calculate  $k_{p,STC}$  for resistive load, Eq. (3.6) of Ch. 3, which explains the impedance operation of boost converter, is utilized and it can be transformed into STC as:

$$R_L = \frac{1}{(1-D)^2} R_{pv\_seen} \Rightarrow STC: R_L = \frac{1}{(1-D_{mpp,STC})^2} R_{mpp,STC} \quad (5.16)$$

Re-arranging the above equation to attain the  $D_{mpp,STC}$ , we get

$$D_{mpp,STC} = 1 - \sqrt{\frac{R_{mpp,STC}}{R_L}} \quad (5.17)$$

At  $D_{mpp,STC}$ , the PV array corresponds to MPP variables under STC conditions, i.e.  $R_{mpp,STC} = V_{mpp,STC}/I_{mpp,STC}$ . Planting these values in above equation, we get

$$D_{mpp,STC} = 1 - \sqrt{\frac{V_{mpp,STC}}{I_{mpp,STC}} \times \frac{1}{R_L}} \quad (5.18)$$

Putting  $D_{mpp,STC}$  value from Eq. (5.18) into Eq. (5.15), we get  $k_{p,STC}$  value for resistive load as:

$$k_{p,STC} = \frac{\sqrt{\frac{V_{mpp,STC}}{I_{mpp,STC}} \times \frac{1}{R_L}}}{V_{mpp,STC}} \quad (5.19)$$

Where,  $V_{mpp,STC}$  is the array voltage and is equal to  $N_s \times V_{mpp\_mod}$ .  $I_{mpp,STC}$  is the array current and is equal to  $N_p \times I_{mpp\_mod}$ .  $N_s$  and  $N_p$  are the number of series and parallel modules respectively in a PV array. While  $V_{mpp\_mod}$  and  $I_{mpp\_mod}$  are the MPP values of voltage and current respectively of the PV module under STC, which can be obtained from Manufacturers datasheet.

To find out the  $k_p$  gain for all weather conditions, assuming  $V_{mpp,STC}$  is to be attained but at different irradiance. Since, irradiance level is majorly reflected in  $I_{pv}$ , Eq. (5.18) can be modified to find the D as:

$$D = 1 - \sqrt{\frac{V_{mpp,STC}}{I_{pv}} \times \frac{1}{R_L}} \quad (5.20)$$

Since  $V_{Ref}$  is equal to  $V_{mpp,STC}$  and taking D from the above relation, Eq. (5.15) can be used to find  $k_p$  as:

$$k_p = \frac{1-D}{V_{mpp,STC}} = \frac{\sqrt{\frac{V_{mpp,STC}}{I_{pv}} \times \frac{1}{R_L}}}{V_{mpp,STC}} \quad (5.21)$$

Taking  $k_p$  and  $k_{p,STC}$  relations from Eqs. (5.19) and (5.21) respectively, the compensation factor 'X<sub>c</sub>' between the two can be formulated as:

$$X_c = \sqrt{\frac{I_{mpp,STC}}{I_{pv}}} \quad (5.22)$$

$$k_p = k_{p,STC} \times X_c = \frac{\sqrt{\frac{V_{mpp,STC}}{I_{mpp,STC}} \times \frac{1}{R_L}}}{V_{mpp,STC}} \times \sqrt{\frac{I_{mpp,STC}}{I_{pv}}} \quad (5.23)$$

For resistive loads,  $k_p$  gain can be tuned using Eq. (5.23) and is valid for all kinds of weather conditions. Eq. (5.23) further reveals two important facts: 1) Since the information of  $V_{mpp,STC}$  and  $I_{mpp,STC}$  (from Manufacturers`s datasheet) and  $R_L$  can be obtained, the only factor required to set the  $k_p$  gain is  $I_{pv}$ , which is the current of PV array at present instant and is measured with the help of current sensor. Hence,  $k_p$  is a dynamic or adaptive gain which will be changed with varying  $I_{pv}$  i.e. varying weather conditions and 2) The formula of  $k_p$  gain contains the  $R_L$  value, which means that  $k_p$  gain depends upon the load value and is different for different resistive loads.

#### 5.4.2.2 Tuning of $k_p$ for battery load

Since battery offers a low resistance (typically in milli-ohms) and absorbs all the available current,  $I_{pv}$  is not producing any major impact. As a result, to find the  $k_p$  gain for battery loads, voltage relation of boost converter can be utilized. Consider  $V_B$  is the nominal voltage of the battery, the voltage relation can be written in STC form as:

$$V_B = \frac{1}{1-D} V_{pv} \Rightarrow STC: V_B = \frac{1}{1-D_{STC}} V_{mpp,STC}(STC) \quad (5.24)$$

Re-arranging the above equation to find  $D_{STC}$

$$D_{STC} = 1 - \frac{V_{mpp,STC}}{V_B} \quad (5.25)$$

Putting  $D_{STC}$  from above relation in Eq. (5.15), we can get  $k_{p,STC}$  as:

$$k_{p,STC} = \frac{1}{V_B} \quad (5.26)$$

Since battery load is not influenced by current, no compensation is required in  $k_{p,STC}$  value under battery load unlike resistive load. Hence,  $k_p$  gain is same:

$$k_p = k_{p,STC} = \frac{1}{V_B} \quad (5.27)$$

The above equation expresses that the only information required to set the  $k_p$  gain is the battery voltage. Since the  $V_B$  value is approximately fixed,  $k_p$  gain under battery load can be considered as static gain.

#### 5.4.2.3 Boundary limits

It can be seen from Fig. 5.7 that the D should be operating within the boundary limits of 0 & 1, otherwise the PV system may become unstable. This implies that:

- Lower Limit (LL):  $D = 1 \Rightarrow$  PV array is operating at  $V_{pv} = 0$  and  $I_{pv} = I_{sc}$ .
- Upper Limit (UL):  $D = 0 \Rightarrow$  PV array is operating at  $V_{pv} = V_{oc}$  and  $I_{pv} = 0$ .

It should be noted that these limits criteria are not considered in details in the literature. However, the scheme presented in this paper provides the facility to check the boundary limits at every instant. Before assigning the new D, MPPT designer can check the boundary limits from the following two limits relations:

$$LL: 1 = D_{prev} - k_p \times error \quad (5.28)$$

$$UL: 0 = D_{prev} - k_p \times error \quad (5.29)$$

These two relations Eq. (5.28) and Eq. (5.29) which are obtained from Eq. (5.9) mathematically explain that since the value of  $k_p$  can be obtained from Eq. (5.23) (for resistive load) and Eq. (5.27) (for battery load) and  $D_{prev}$  is known, the designer can find out the magnitude of errors which drag the D to limits.

## 5.5 Simulation results and comparative study

Figure 5.8 shows the PV array that is exposed to three different types of shading patterns. To evaluate the comparative performance between different techniques, MPPTs are applied to PV array in Matlab/Simulink environment. The simulations are carried out using the comprehensive PV model developed in [32]. PV array contains four strings and each of them contains four modules, i.e. 4 x 4. The 55 W PV module [33] is used whose electrical specifications are given in Table 1.1. Each

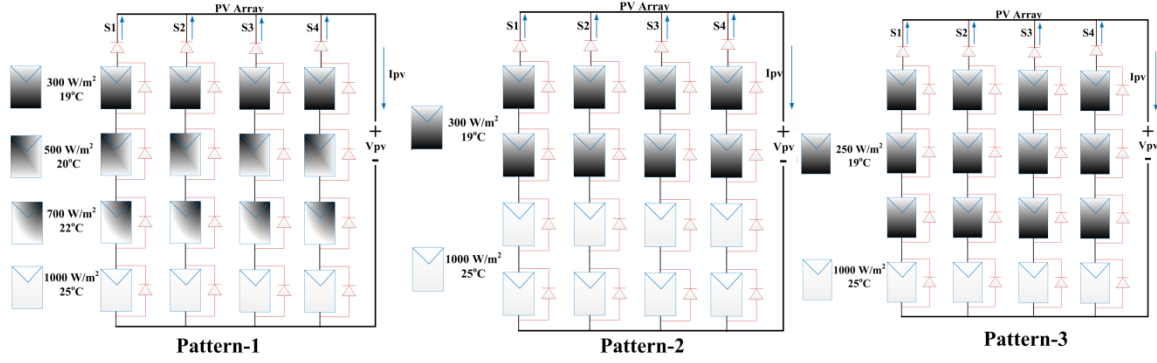


**Figure 5.8** – PV array with three distinct shading patterns

PV module contains a single bypass diode. As  $N_S = 4$  and  $N_{BD,M} = 1$ , so three voltage parameters for the current PV array are configured as:

$$\Delta V = \frac{V_{OC,Array}}{4} \quad (5.30)$$

$$\Delta V_{1st} = \frac{\Delta V}{2} = \frac{V_{OC,Array}}{8} \quad (5.31)$$

$$V_{LIM} = 3 \times \Delta V + \Delta V_{1st} = \frac{7 \times V_{OC,Array}}{8} \quad (5.32)$$

In R-MPP loop, voltage step of 1 V is utilized for P&O method. In the following discussion, the performance of techniques are presented, when PV array exhibits different position of GM: in the initial part (Pattern-1), in the middle (Pattern-2) and in the last part (Pattern-3) of the PV curve.

MPPT presented in [73] is a load line based technique, which detects the GM vicinity with simple load line relation i.e.  $V_{Ref} = \frac{N_S \times V_{OC}}{N_p \times I_{SC}} I_{PV}$ . On the other hand, in order to detect the GM vicinity, the technique presented in [74] always scans the complete PV curve by perturbing the voltage of the array at integral multiples of  $0.8 \times V_{OC,M}$ . It should be noted that the proposed BD-MPPT and other two algorithms [73-74] detect the GM vicinity by perturbing the voltage of the PV array. As a consequence, the convergence speed of each algorithm depends upon the computations of voltage perturbations. Fig. 5.9 shows the tracking ability for each algorithm under three different shading patterns shown in Fig. 5.8.

It can be seen that under pattern-1, proposed technique executes five operating

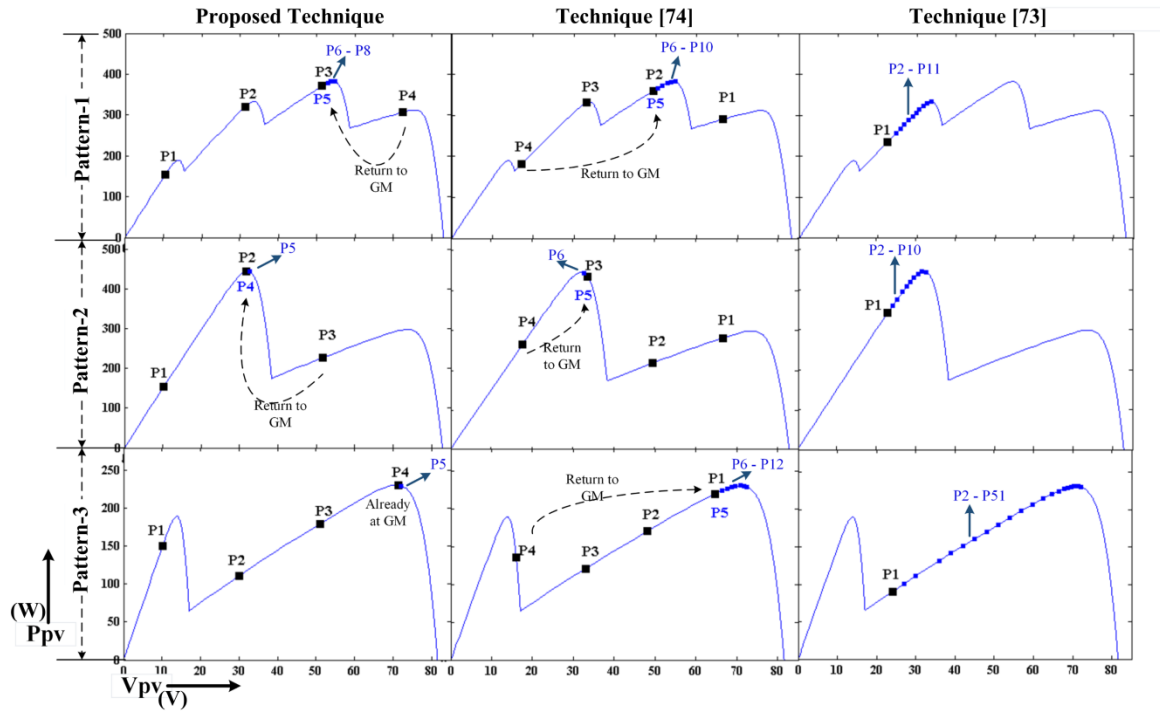


**Figure 5.9** – Comparative performance of MPPTs – Three distinct shading patterns

points (P1→P2→P3→P4→P5) to detect the GM vicinity and three points (P6→P7→P8) in R-MPP loop to reach the GM precisely. On the other hand, technique [74] also executes five points to detect the GM vicinity and further executes four points to reach GM. However, the technique [73] executes single point (P1) to detect the GM vicinity while it executes ten points to reach the GM. The performance of all these techniques is summarized in Table 5.1.

It can be seen from Table 5.1 that voltage perturbations column of each technique contains two values. For instance, under pattern-1, proposed technique has

**Table 5.1** – Comparative performance of MPPTs – Three distinct shading patterns

Pattern	Ideal Power (W)	Techniques	Voltage Perturbations	GM Detection	Power Attained
1	383.83	Proposed	5 + 3 = 8	Yes	383.81
		MPPT [74]	5 + 5 = 10	Yes	383.81
		MPPT [73]	1 + 10 = 11	No	333.1
2	445.5	Proposed	4 + 1 = 5	Yes	445.5
		MPPT [74]	5 + 1 = 6	Yes	445.4
		MPPT [73]	1 + 9 = 10	Yes	445.3
3	231.0	Proposed	4 + 1 = 5	Yes	231.0
		MPPT [74]	5 + 7 = 12	Yes	231.0
		MPPT [73]	1 + 50 = 51	Yes	230.9

the following entry:  $5 + 3 = 8$ , where 5 represent the number of voltage perturbations to detect the GM vicinity and 3 indicates the voltage steps to reach GM precisely from GM vicinity. Table 5.1 shows that under pattern-1, technique [73] is not able to detect the GM and is trapped in one of the LM, which can also be confirmed from Fig. 5.9. As a result, this technique extracts less amount of power from the PV array compared to the other two techniques. On the other hand, Table 5.1 indicates that the proposed technique and technique [74] are very accurate in locating the GM. However, the proposed technique always consumes less voltage steps compared to the technique [74] and technique [73]. This highlights the superior tracking ability of the proposed technique as compared to others.

## 5.6 Modifications and integration of techniques

After proving the effectiveness of the proposed BD-MPPT, the technique is further improved which is explained in this section. It is pertinent to note that the basic philosophy and voltage relations of the technique remains the same, however the design principles are modified in such a way that the technique should perform less voltage perturbations to detect the GM. Also, the technique behaves efficiently when PV array is under uniform conditions. Furthermore, the new modification should provide the facility to the MPPT designer that it can be integrated with the MPPT designed in Ch. 4 i.e. MPPT for uniform conditions. It should be noted that the proposed BD-MPPT scheme has already been published and is given the Ref [40] in the reference list. From here onwards, the discussion contains the modified MPPT which is the improved form of MPPT [40], which is designed in Sec. 5.3.

### 5.6.1 Predictive current based modification and $I_{sc}$ measurement

Figure 5.10 shows the complete flowchart of the modified technique. It can be seen that initially, the technique measures short-circuit current ( $I_{sc}$ ) along with  $V_{oc}$ .  $I_{sc}$  is measured in order to evaluate that the PV array is under uniform condition or partial shading.  $I_{sc}$  is not measured by short-circuiting the PV array directly, instead it will be measured using a large value capacitor in parallel with PV array as shown in Fig. 5.11. Initially, a fully discharge capacitor behaves like a short- circuit and large value

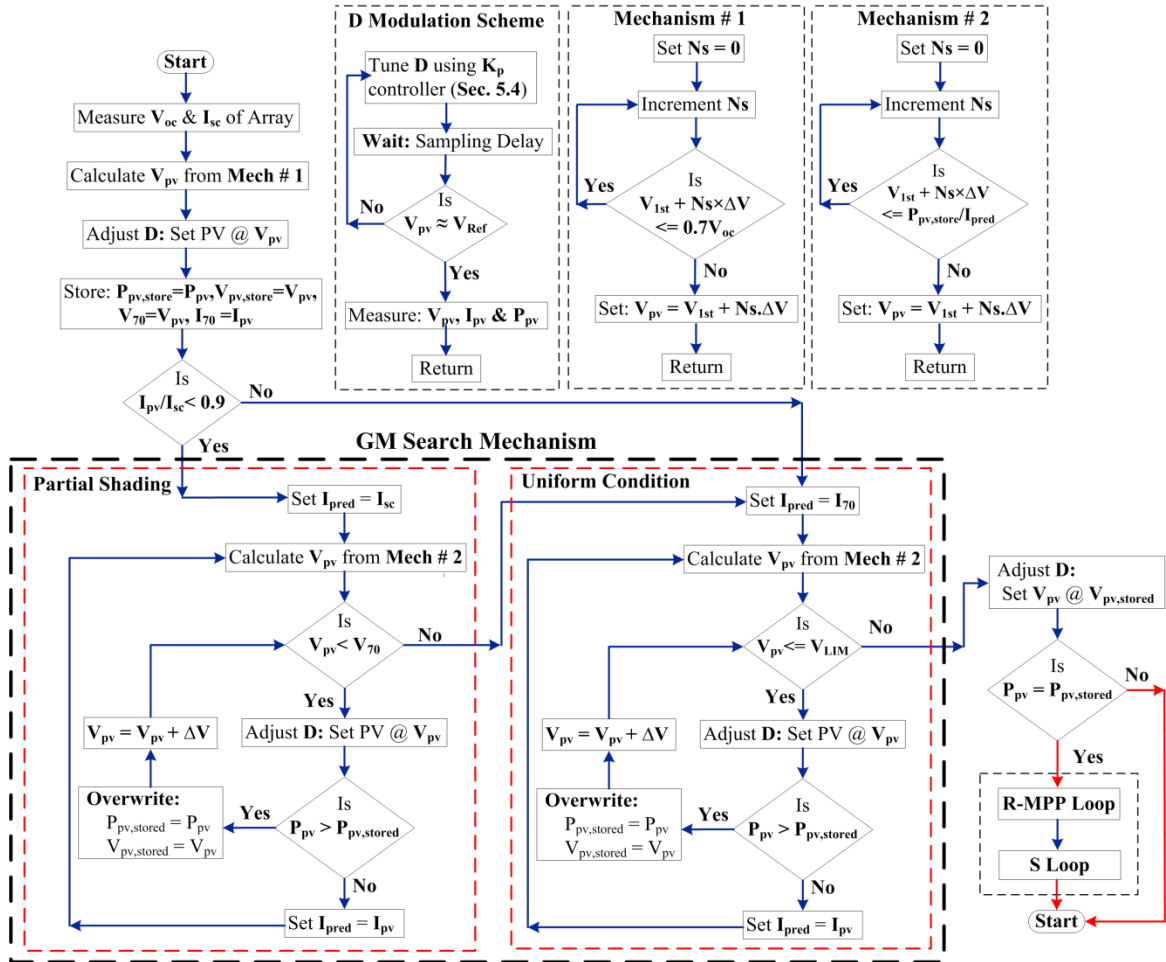


Figure 5.10 – Improved GM search mechanism stage of modified MPPT

of capacitor ensures that it has slow charging rate. Consequently,  $I_{sc}$  can be measured without short-circuiting the array. The capacitor, which is used to measure the  $I_{sc}$ , is also connected in parallel with a resistor, such that stored energy in the capacitor can be dissipated through resistor before next measurement of  $I_{sc}$ . After measuring  $I_{sc}$ , the

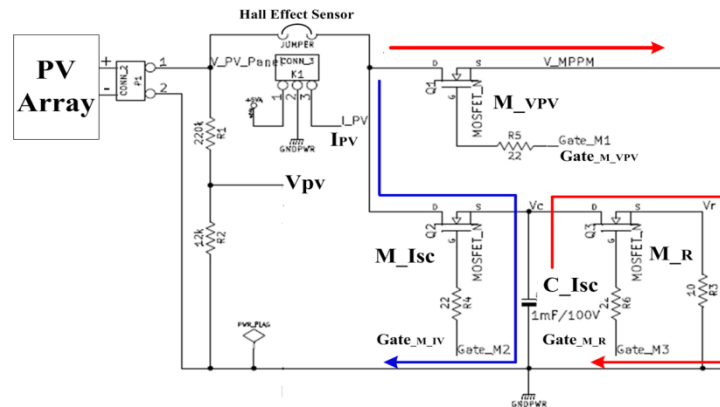


Figure 5.11 – Circuit arrangement to measure  $I_{sc}$

the algorithm calculates the  $V_{pv}$  which is near to  $0.7 \times V_{oc}$ . Normally, the  $V_{mpp}$  is at 0.75 to 0.85 fraction of  $V_{oc}$ . However, a cautious threshold value (0.7) is set. The  $V_{pv}$  is calculated through Mechanism-1 as shown in Fig. 5.10, where it can be seen that the mechanism utilizes the same voltage relations ( $V_{1st}$ ,  $\Delta V$ ) which are designed in Sec. 5.3.1. The  $V_{1st}$ ,  $\Delta V$  and  $V_{LIM}$  are designed keeping in view the activation of bypass diodes and occurrence of LMs on I-V curve. Since the modified scheme utilizes the same voltage steps in its formulation, therefore, the ability of algorithm to evaluate the PV at constant current regions (CCRs) between mini-I-Vs will remain intact. The Mechanism-1 contains a simple principle:

Step-1: Increment  $N_s$

Step-2: Is  $(V_{1st} + N_s \times \Delta V) \leq 0.7V_{oc}$

Step-3: Yes - Goto to Step-1 / No - Set  $V_{pv} = V_{1st} + N_s \times \Delta V$  and Return

After determining  $V_{pv}$ , the D modulation scheme takes control in order to set the operating voltage of PV array at desired  $V_{pv}$ . The modulation scheme is already explained in detail in Sec. 5.4. When PV array starts operating at  $V_{pv} = 0.7V_{oc}$ ,  $I_{pv}$  of array is measured, and array condition is evaluated with the ratio  $I_{pv}/I_{sc}$  as shown in Fig. 5.10. It should be noted during uniform conditions, when PV array is operating at  $V_{pv} = 0.7V_{oc}$ ,  $I_{mpp}$  is at fraction of  $I_{sc}$ , which normally varies from 0.85 to 0.9. Hence, 0.9 value is selected to be on the safe side. Therefore, if ratio is less than 0.9, it means that there is a significant drop in  $I_{pv}$  of array, indicating partial shading. Otherwise, the technique considers that the PV array is under uniform condition. Both uniform condition loop and partial shading loop belongs to the GM search mechanism as shown in Fig. 5.10. It is pertinent to note that modified MPPT and MPPT [40] used the same voltage relations ( $V_{1st}$ ,  $\Delta V$  and  $V_{LIM}$ ) and R-MPP loop & S-loop, the main difference between two schemes is the GM search mechanism along with detection of two conditions (uniform or partial shading) through  $I_{sc}$ . Hence, the modified scheme is expected to perform better by consuming less voltage perturbations in its GM search mechanism to detect the GM vicinity.

In case of partial condition loop, the algorithm simply sets the  $I_{pred}$  equals to the  $I_{pv}$  measured at  $0.7V_{oc}$  ( $V_{70}$ ). It should be noted, according to P-5 of Sec. 5.2, the  $I_{pv}$  of present  $V_{pv}$  of array remains the same or falls at higher voltage values. Since

algorithm always scan the I-V curve from left side, it will consider the  $I_{pv}$  of present  $V_{pv}$  remains the same at higher  $V_{pv}$  values. As the first sample is executed at  $0.7V_{oc}$ , the algorithm stores the power and sets the  $I_{pred} = I_{70}$ . After that, instead of taking voltage step, the algorithm finds out the  $V_{pv}$ , which gives more power through Mechanism-2 as shown in Fig. 5.10. For instance, first power is sampled at  $V_{70}$  and its respective values are stored i.e.  $P_{pv,store} = P_{70}$  and  $I_{pred} = I_{70}$ . Considering, the current of array remain the same, the voltage at which we can expect greater  $P_{pv}$  can be found as:

$$I_{pred} \times V_{Ref} > P_{pv,store} \quad (5.33)$$

$$V_{Ref} > \frac{P_{pv,store}}{I_{pred}} \quad (5.34)$$

As already described, the aim of the algorithm is to evaluate the I-V curve on CCR, same voltage steps are used to find  $V_{Ref}$ . Eq. (5.34) can be modified as:

$$V_{1st} + N_s \times \Delta V > \frac{P_{pv,store}}{I_{pred}} \quad (5.35)$$

Likewise Mechanism-1, Mechanism-2 can be sequenced as:

Step-1: Increment  $N_s$

Step-2: Is  $(V_{1st} + N_s \times \Delta V) \leq (P_{pv,store} / I_{pred})$

Step-3: Yes - Goto to Step-1 / No - Set  $V_{pv} = V_{1st} + N_s \times \Delta V$  and Return

After setting the array at  $V_{pv}$  through D-modulations scheme, if  $P_{pv}$  of current sample is greater, the algorithm overwrites the stored values, i.e. ( $V_{pv,store}$  and  $P_{pv,store}$ ) with new values and take the voltage step ( $+\Delta V$ ) as shown in Fig. 5.10. Otherwise, the algorithm updates the  $I_{pred}$  with the current sample of  $I_{pv}$  and find the  $V_{pv}$  of next iteration through Mechanism-2. This process is completed until the algorithm finds out that the  $V_{pv}$  reach the  $V_{LIM}$ , the limit voltage upto which the PV curve needs to be scanned. After that, the algorithm returns to GM vicinity by setting the  $V_{pv}$  at stored value. After that, algorithm enters to R-MPP loop to detect the GM/MPP precisely. After that, the algorithm enters into S-loop, where it remains stick to MPP unless the condition changes.

Under uniform condition loop, the algorithm sets the  $I_{pred}$  equal to  $I_{sc}$  and the

whole process is same as already discussed previously. This can be confirmed from the flowchart shown in Fig. 5.10. However, the only exception is that the algorithm breaks this loop, and enters in to partial shading loop, when  $V_{pv}$  becomes equal to  $V_{70}$  of PV array. As the algorithm takes the first sample at  $V_{70}$ , therefore, information of  $I_{70}$  is available. Hence, initially algorithm finds the next  $V_{pv}$  by setting  $I_{pred}$  equals to  $I_{70}$  in partial shading loop, and the process is repeated until the algorithm reaches the  $V_{LIM}$ .

### 5.6.2 Integration of techniques

It can be seen that the GM search mechanism stage in Fig. 5.10 is followed by R-MPP and S-Loop. Hence, the E-MPP loop of MPPT (developed in Ch. 4) can be added to integrate the two techniques as shown in Fig. 5.12.

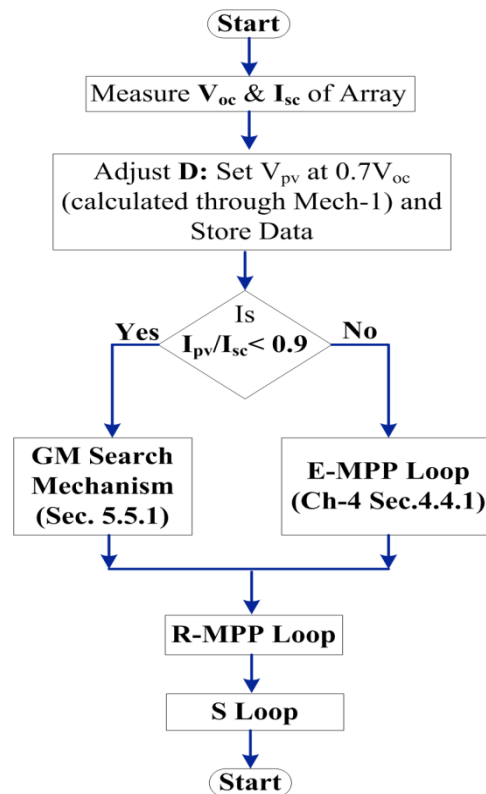
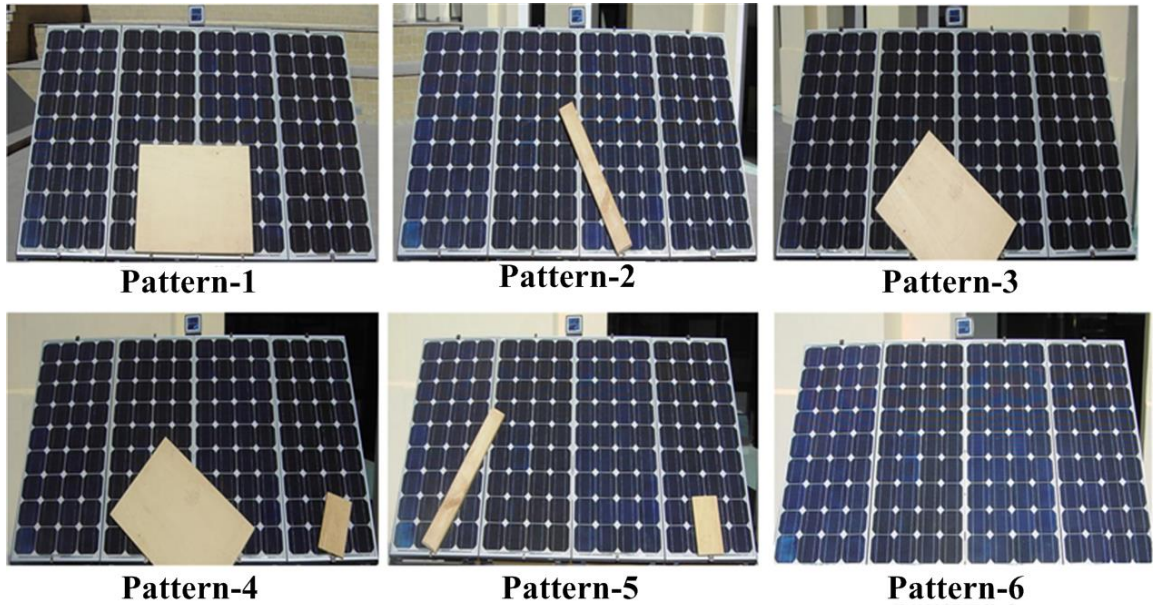


Figure 5.12 – Integration of uniform and shading MPPTs

### 5.6.3 Experimental setup, results and discussion

In order to confirm the effectiveness of MPPTs, the MPPT [40] and modified scheme are applied to PV array, which is subjected to six different partial shading patterns as shown in Fig. 5.13. The apparatus used to perform experiments has already



**Figure 5.13** – PV array with six different partial shading patterns

been explained in detail in Sec. 4.7 of Ch-4. The description about the hardware components is displayed in Table 4.4 of the same chapter. The sampling rate of PV system is set at 5 ms. The battery of 48 V is connected as load. Both techniques used the same D-modulation scheme (explained in Sec. 5.4) and  $\text{Error} = V_{\text{Ref}} - V_{\text{pv}}$  is set with tolerance of  $\pm 0.5$  V. Both techniques process the R-MPP loop and S-loop in the same as that of the MPPT designed in Ch. 4. However, in R-MPP loop, both techniques execute the small perturbations with a step size of 1V i.e.  $\Delta V = 1V$ .

### 5.6.3.1 Results and discussion

Figure 5.14 illustrates the standard format of the evaluation of techniques when PV array is subjected to Pattern-1. Upper graph (a) shows the behavior of modified MPPT while lower graph (b) displays the behavior of MPPT [40]. It can be seen, that initially I-V curve is scanned for 10 ms to detect the ideal MPP. After that, the duty cycle of techniques is set at 90%, i.e.  $D_{\text{in}} = 0.9$  and techniques take the control. Initially, both schemes measure  $V_{\text{oc}}$  as indicated in Fig. 5.14 to set the values  $V_{\text{1st}}$ ,  $\Delta V$  and  $V_{\text{LIM}}$ . While, modified scheme also measures  $I_{\text{sc}}$  in its operation to differentiate between the partial and uniform condition. Fig. 5.14 shows that the modified scheme consumes 3 samples (large  $\Delta V$ ) in its GM search mechanism to detect the GM vicinity, while scheme [40] takes 5 samples in its GM search mechanism. Since, both

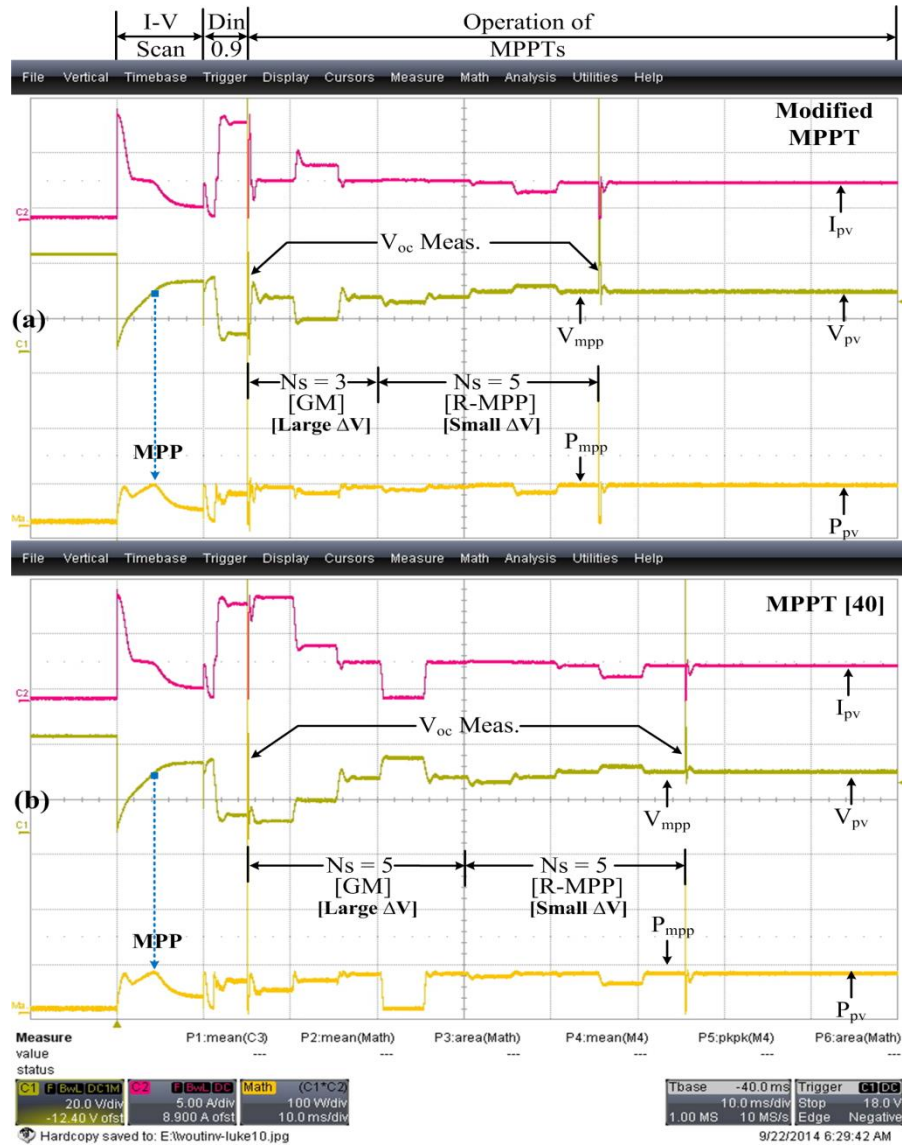
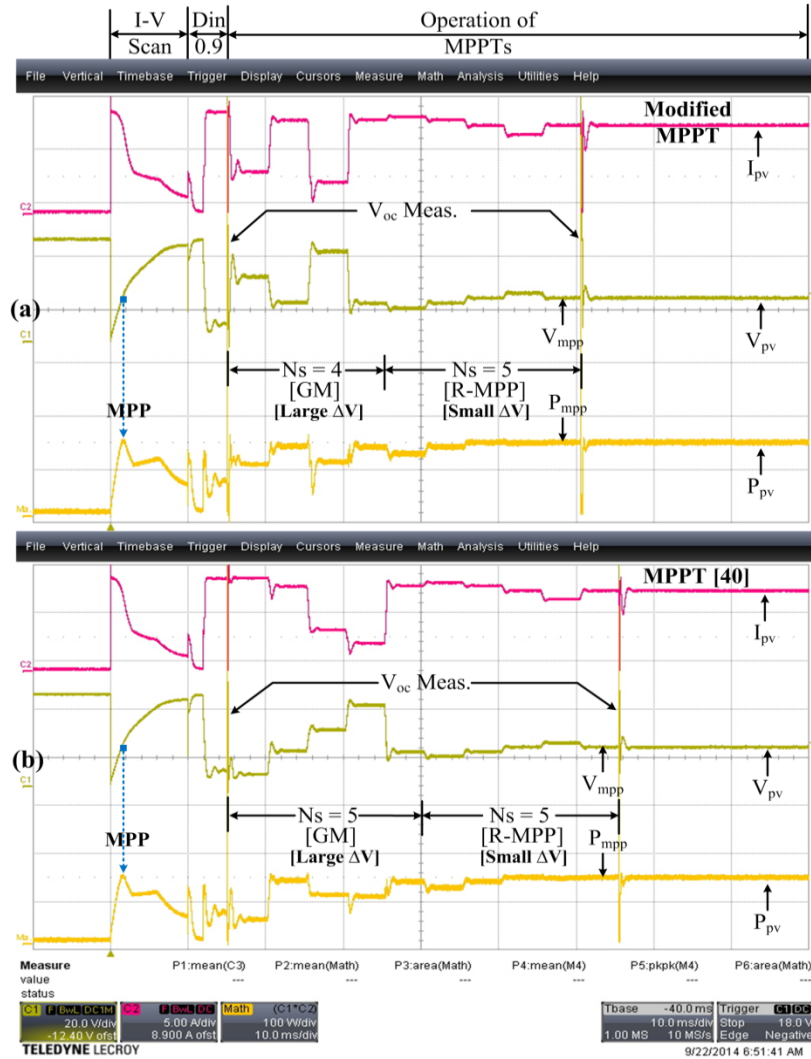


Figure 5.14 – Performance of MPPTs when PV array is under Pattern-1

techniques used the same R-MPP loop with same  $\Delta V$  steps ( $\Delta V = 1V$ ), both MPPTs execute 5 samples to detect the real MPP (small  $\Delta V$ ). After that, both techniques again measure  $V_{oc}$  to detect that weather condition. As weather condition is not changed, both MPPTs enter into S-loop, where they will stick to MPP until the weather changes.

Figure 5.15 illustrates the performance of two techniques under Pattern-2. Once again, the modified scheme executes 1 sample less compared to the MPPT [40] to detect the GM. This will give an advantage of 5 ms for modified MPPT as techniques have a sampling rate/delay of 5 ms. Hence, less voltage perturbations



**Figure 5.15** – Performance of MPPTs when PV array is under Pattern-2

means fast tracking ability of the algorithm. While, both technique executes same  $\Delta V$  steps in R-MPP loop.

When PV array is operating under Pattern-3, it exhibits two peaks of similar power values as shown in Fig. 5.16. The modified scheme executes two samples to detect the GM vicinity, while MPPT [40] is not able to detect the true GM vicinity and is caught in the LM vicinity. Because both schemes work in different peaks, as a result, proposed scheme executes 3-sample in R-MPP loop while MPPT [40] utilizes 4 samples. Consequently, the overall advantage of the proposed scheme is 20 ms as it consumes 4 samples ( $2+3=5$ ) less than the scheme [40] ( $5+4=9$ ).

Figures 5.17 and 5.18 show the superior performance of modified MPPT in locating the GM compared to MPPT [40] when PV array is partially shaded with

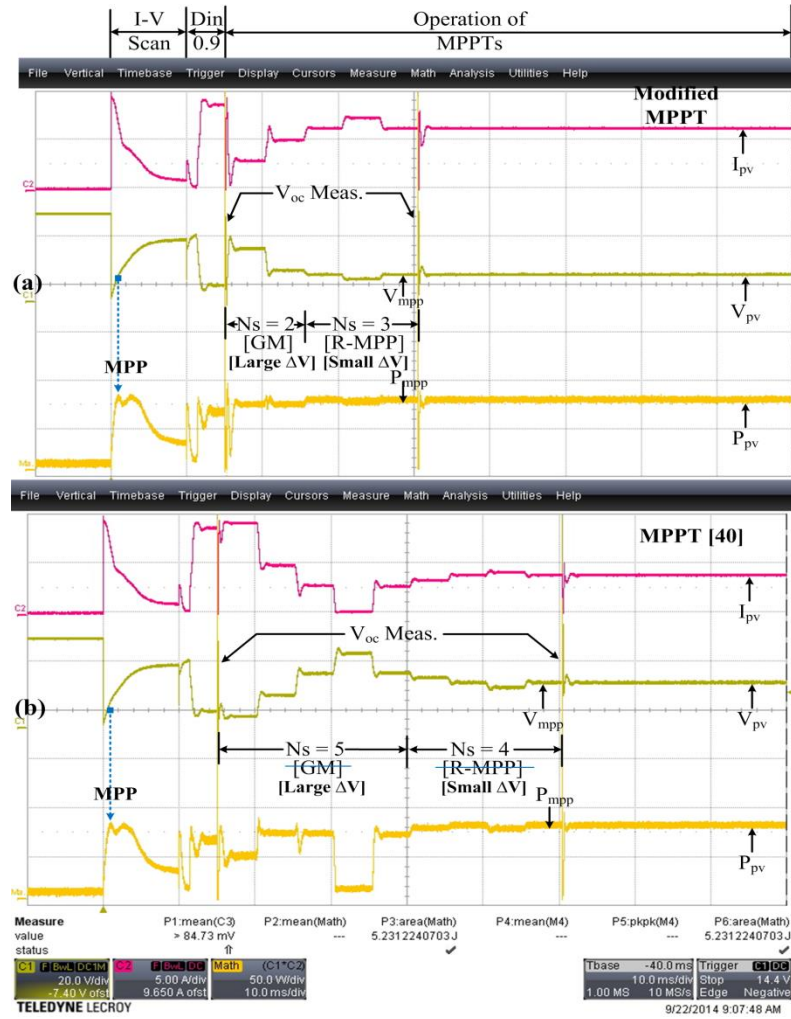


Figure 5.16 – Performance of MPPTs when PV array is under Pattern-3

Pattern-4 and Pattern-5, respectively. While, Fig. 5.19 displays the behavior of two techniques when PV array is under Pattern-6 i.e. uniform condition. It can be seen from Fig. 5.19, that the proposed scheme executes 3 perturbations to detect the GM. The effectiveness of the modified MPPT can be realized from the Arrow-1 position in Fig. 5.19(a), where at second  $\Delta V$  step, the technique experiences a heavy dip in  $I_{pv}$  of array. This phenomenon is occurred because  $V_{pv}$  moves from MPP region to slope region, where  $I_{pv}$  falls abruptly. Hence, the technique will return back to MPP region in next perturbation. On the other hand, MPPT [40] experiences the same dip in  $I_{pv}$  as indicated by Arrow-2 in Fig. 5.19(b). But, it executes two more  $\Delta V$  steps compared to modified MPPT. This highlights the efficient tracking ability of algorithm under uniform condition compared to MPPT [40].

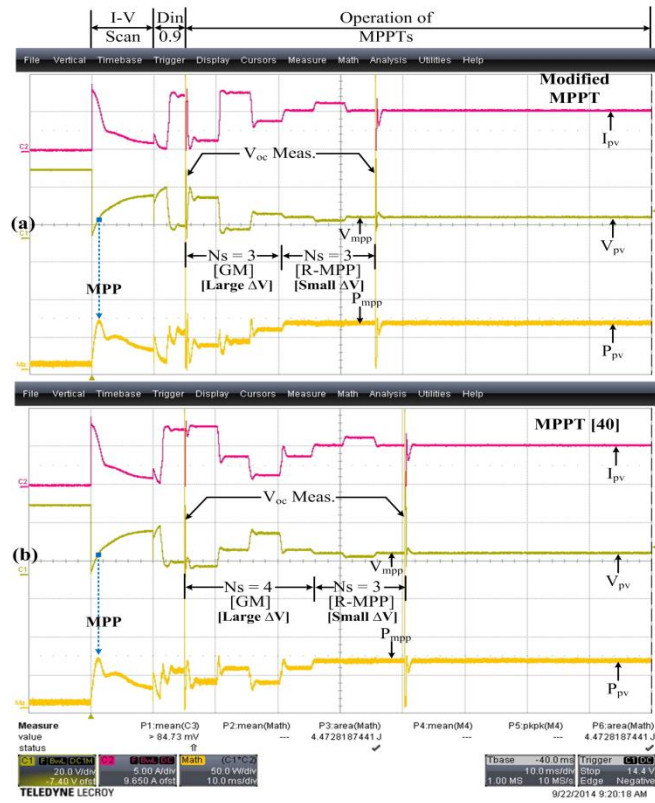


Figure 5.17 – Performance of MPPTs when PV array is under Pattern-4

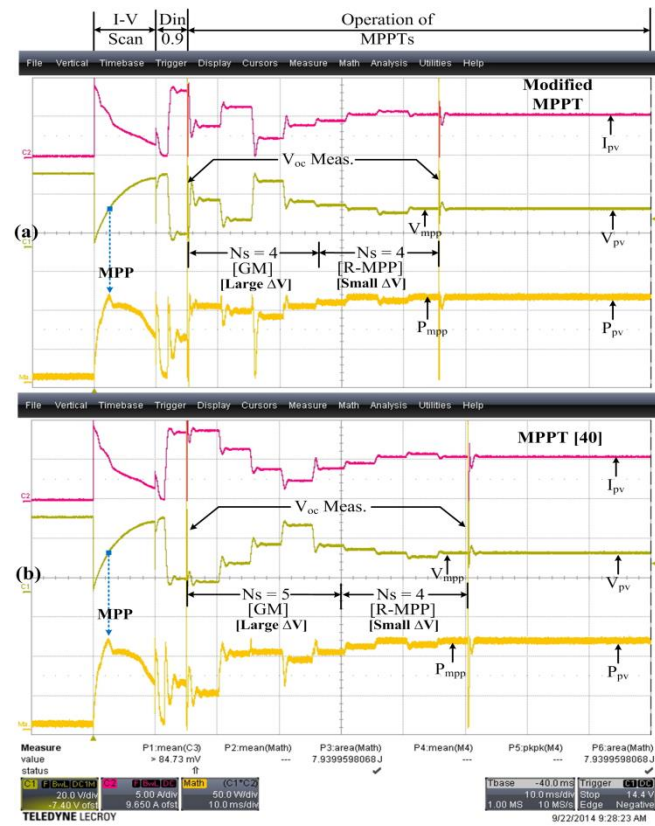


Figure 5.18 – Performance of MPPTs when PV array is under Pattern-5

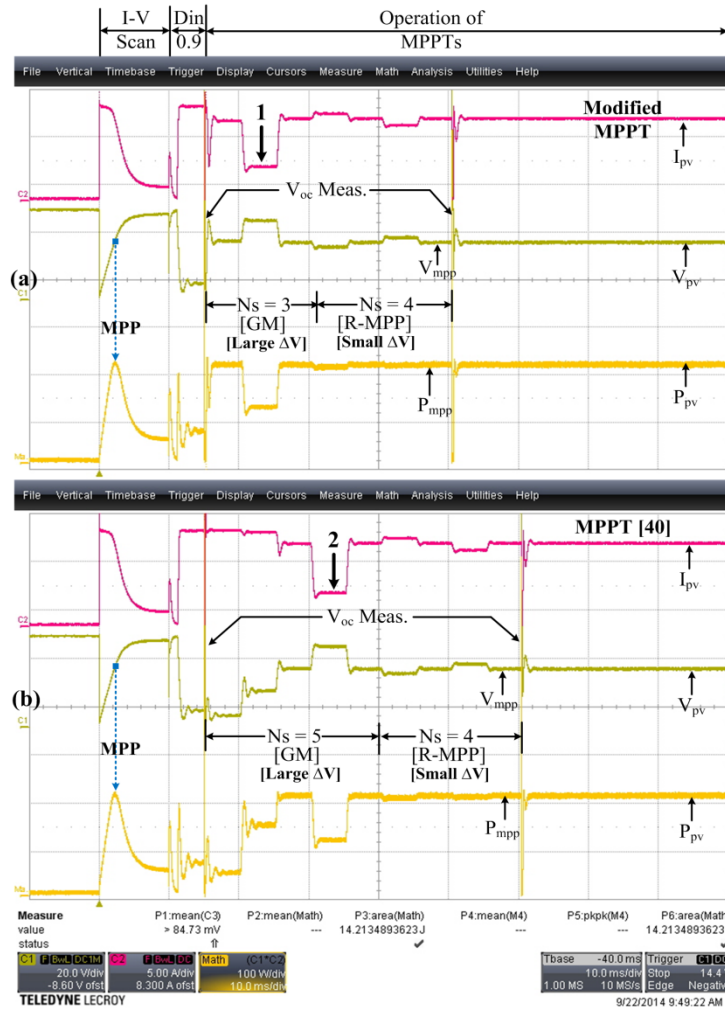


Figure 5.19 – Performance of MPPTs when PV array is under Pattern-6

Table 5.2 – Time response ( $T_R$ ) comparison between MPPTs

Pat.	MPPTs	PV Array				Parameters of Techniques				
		T (°C)	$I_{sc}$ (A)	$V_{mpp}$ (V)	$P_{mpp}$ (W)	GM Det.	Ns GM	Ns MPP	$D_{mpp}$	$T_R$ (ms)
1	Modified	23.6	9.88	21.82	77.1	Yes	3	5	0.567	40ms
	MPPT[40]	23.6	10.1	22.19	74.5	Yes	5	5	0.559	50ms
2	Modified	30.2	9.085	17.25	139	Yes	4	5	0.697	45ms
	MPPT [40]	30.2	9.45	17.62	142.5	Yes	5	5	0.689	50ms
3	Modified	27	9.52	11.08	75.9	Yes	2	3	0.801	25ms
	MPPT [40]	27	9.44	10.87	74.3	No	5	4	0.655	45ms
4	Modified	27.2	8.04	11.39	63.2	Yes	3	3	0.798	30ms
	MPPT [40]	27.2	8.103	11.16	61.3	Yes	4	3	0.794	35ms
5	Modified	27.3	9.06	19.66	109.1	Yes	4	4	0.629	40ms
	MPPT [40]	27.3	9.23	19.95	112.7	Yes	5	4	0.626	45ms
6	Modified	27.1	9.92	25.69	212.7	Yes	3	4	0.551	35ms
	MPPT [40]	27.1	9.85	25.42	210.4	Yes	5	4	0.553	45ms

The tracking ability of modified MPPT compared to MPPT [40] is summarized in Table 5.2. It can be evaluated from the table that the modified MPPT has always tracked the GM vicinity and MPP in less voltage perturbations. This highlights the faster convergence speed of modified MPPT compared to MPPT [40].

### 5.6.3.2 Comparison between modified MPPT and P&O

To further prove the ability of the modified MPPT and inability of P&O to detect the GM, consider Fig. 5.20 where the curves are captured for 10s using the sophisticated oscilloscope. The spikes in  $V_{pv}$  and  $I_{pv}$  indicate the measurement of  $V_{oc}$  and  $I_{sc}$ . It can be noticed that initially, for 2s, uniform conditions are maintained. After 2s, the PV array is shaded manually with an artificial shade as shown in Fig. 5.21. The disturbance due to the placement of artificial shade is indicated in Fig. 5.20 as noise, although the technique continues its operation. When PV array is under uniform

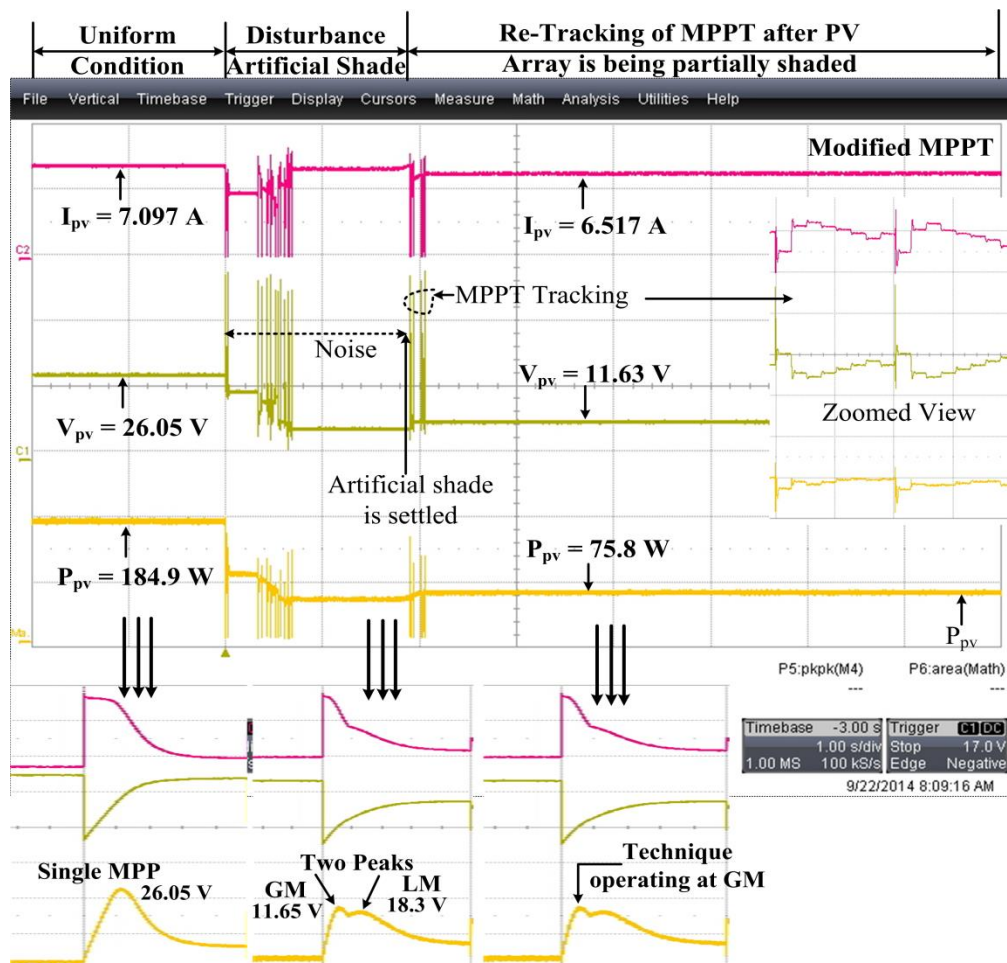


Figure 5.20 – Tracking ability of modified MPPT under variable weather conditions



**Figure 5.21** – PV array is partially shaded with the help of wooden board

condition, the only MPP lies at 26.05 V as shown in the lower graph of Fig. 5.20, which is small in size. The technique is able to operate the PV array at  $V_{pv} = 26.05$  i.e. MPP. After that, when PV array is partially shaded, it exhibits two peaks: one at 11.65 V which is GM and other one is at 18.3 V which is LM as shown in second small graph. Fig. 5.20 displays that when the artificial shade is settled as indicated by arrow, the technique re-initiate its MPP tracking process. The technique is able to locate the GM as it starts operating the  $V_{pv}$  of array at new point i.e.  $V_{pv} = 11.63$  V.

On the other hand, Fig. 5.22 shows that initially, when PV array is under uniform condition, P&O is able to detect the MPP. Under this condition, P&O sets the  $V_{pv}$  of array at 26.89 V, which is approximately the  $V_{pv}$  of MPP point as indicated in lower small graph. But, when PV array is partially shaded with the same shade shown in Fig. 5.21, it exhibits two peaks as shown in second small graph: 1) GM at  $V_{pv} = 11.77$  V and LM at  $V_{pv} = 16.8$  V. It can be seen from Fig. 5.22 that when PV array is partially shaded, P&O sets the operating voltage of the PV array at  $V_{pv} = 16.01$  V which is close to the  $V_{pv} = 16.86$  V of LM. As a result, PV array is caught in the LM and generates less power due to P&O algorithm. Thus indicating the inability of P&O to detect the GM during partial shading conditions.

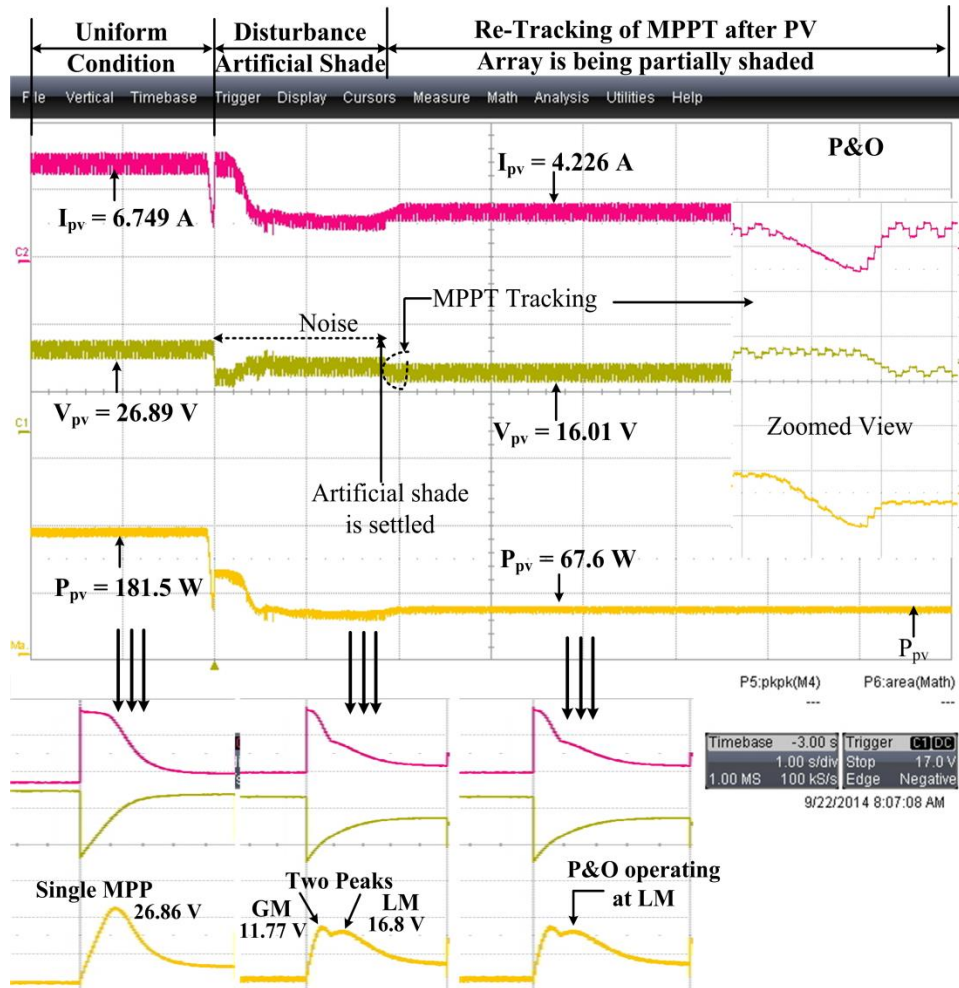


Figure 5.22 – Tracking ability of P&O against variable weather conditions

### 5.6.4 Experimental validation on large PV array

To further prove the effectiveness of the modified MPPT over the MPPT [40], experimental data of a building integrated PV (BIPV) plant has been recorded which is installed in Italy. The plant contains 352 PV modules, which are arranged in the form of 16 strings. Each string contains 22 modules. Each PV module is made from single crystalline silicon technology and contains 3 bypass diodes. At STC, PV module has maximum power  $P_{MPP} = 245$  W which corresponds to voltage  $V_{MPP} = 30.3$  V and current  $I_{MPP} = 8.09$  A, therefore the PV plant is able to produce 86.24 kW. This PV plant is affected by natural shades from architectural elements like tie-beams on the shed roof. Since the nature of the shades is continuously changing with the variation of sun's parameters (irradiance and position), therefore the PV plant faces

different partial shading patterns with different irradiance levels at different periods. Experimental data of three different occasions has been recorded with the aid of advanced data acquisition system of the PV plant [79]. All the data have imported into Matlab where both techniques have been programmed to apply on it. Finally, all these cases are summarized.

Concerning the current PV plant, where  $N_s = 22$  and  $N_{BD,M} = 3$ , the technique configures the voltage parameters as:

$$\Delta V = \frac{V_{OC,Array}}{22} \times \frac{1}{3} = \frac{V_{OC,Array}}{66} \quad (5.36)$$

$$\Delta V_{1st} = \frac{\Delta V}{2} = \frac{V_{OC,Array}}{132} \quad (5.37)$$

$$V_{LIM} = ((3 \times 22) - 1) \times \Delta V + \Delta V_{1st} = \frac{131 \times V_{OC,Array}}{132} \quad (5.38)$$

#### 5.6.4.1 Case-1: At 10:32 AM and irradiance of 484 W/m<sup>2</sup>

In the morning at 10:32 AM, the sun provides irradiance of 484 W/m<sup>2</sup>. P-V curve of PV plant is shown in Fig. 5.23 along with behavior of MPPT [40] and

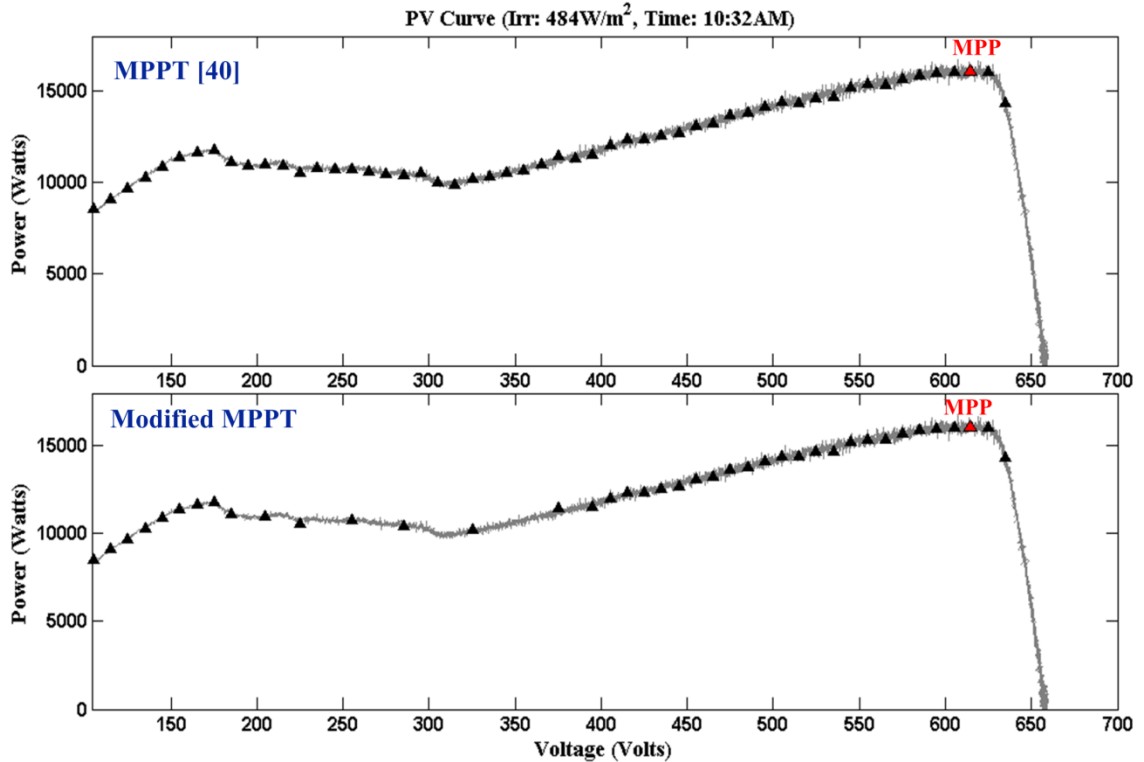


**Figure 5.23** – Response of MPPTs under partially shaded BIPV array at 10:32AM

modified MPPT. The performance of techniques are presented in the form of  $\Delta V$  steps.  $\Delta V$  are indicated using the ‘triangle’ symbol. It can be seen that the MPP is present in the last part of the P-V curve and both techniques are able to detect the GM. However, the modified MPPT executes 51 voltage perturbations compared to 65 perturbations executed by MPPT [40], thanks to  $I_{pv}$  prediction method used in GM search mechanism stage of modified MPPT.

#### 5.6.4.2 Case-2: At 11:01 AM and irradiance of 567 W/m<sup>2</sup>

The behavior of PV plant is shown in Fig. 5.24. Under these conditions, GM occurs at the initial part of the P-V curve. It can be seen from Fig. 5.24 although the MPPT [40] locates the GM vicinity quite early at  $\approx 230$  V. However, it continues to scan the P-V curve up to almost final part due to  $V_{LIM}$  mechanism and executes 65 samples. By close investigation, Fig. 5.24 reveals that the two peaks (indicated by arrows) are of similar powers. While, they occurred at much different voltages, i.e. one at  $\approx 230$ V and other at  $\approx 625$ V. On the other hand, the modified MPPT executes far less samples and just executes 36 perturbations to detect the GM.

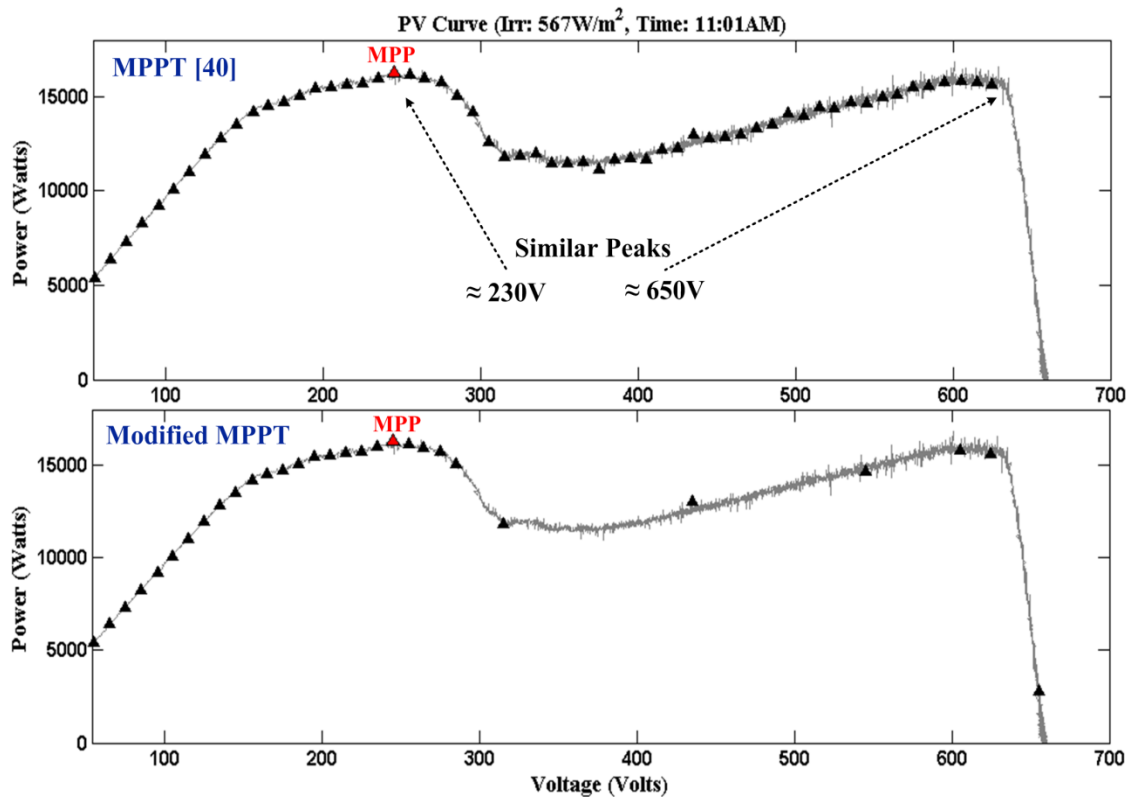


**Figure 5.24** – Response of MPPTs under partially shaded BIPV array at 11:01AM

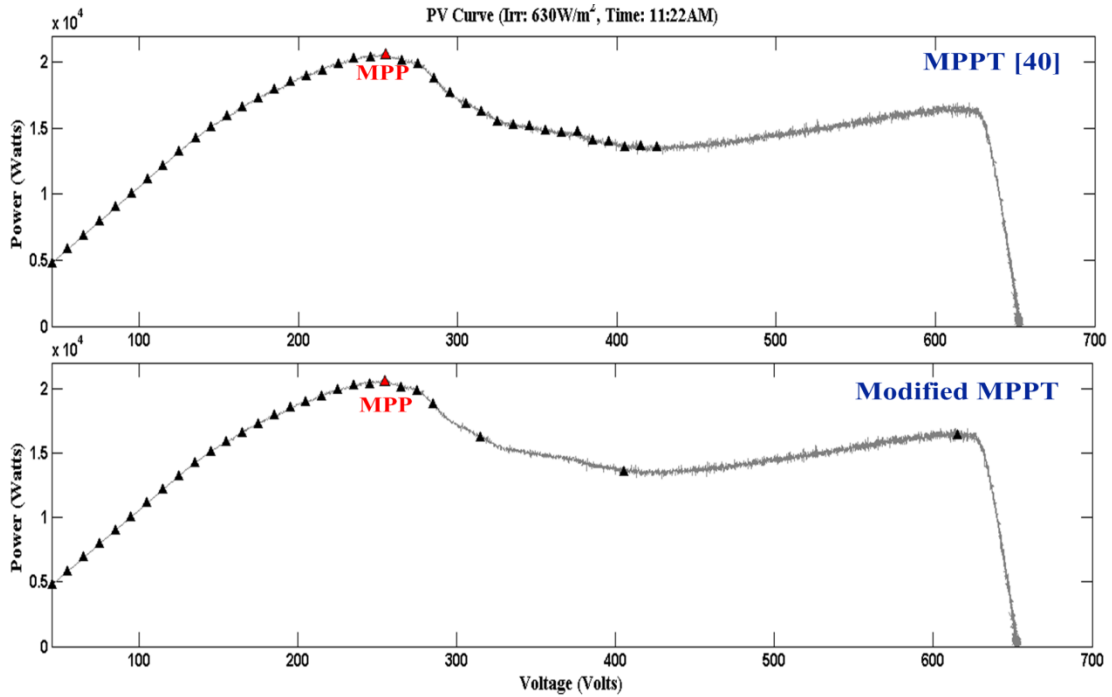


**Figure 5.25** – Response of MPPTs under partially shaded BIPV array at 11:22AM

#### 5.6.4.3 Case-3: At 11:22 A.M and irradiance of 630 W/m<sup>2</sup>

Response of plant at 11.22 A.M is shown in Fig. 5.25, In this case, again MPPT [40] identifies the GM vicinity at the early part of the P-V curve. This time, the technique does not scan the P-V curve upto same voltage as in case-2. This reveals the adaptive ability of the MPPT [40]. In this case, technique [40] stops the scanning in between (courtesy  $V_{LIM}$ ) because the last peak is not producing the power close to GM. Thus skipping almost one-third of the P-V curve. However, even in this case, the modified MPPT executes less voltage perturbations to detect the GM.

#### 5.6.4.4 Summary

The summary of three cases discussed above is shown in Table 5.3. Where, it can be seen that the modified MPPT outperforms MPPT [40] on each and every case.

**Table 5.3** – Comparison between MPPTs using dataset of large PV array

Cases	Irradiance (W/m <sup>2</sup> )	Time (AM)	Proposed		MPPT [40]	
			GM	Ns	GM	Ns
1	484	10:32	Yes	51	Yes	65
2	567	11:01	Yes	36	Yes	65
3	630	11:22	Yes	33	Yes	45

# Chapter 6

## Conclusions

In this thesis, initially, the effects of weather conditions and loads on photovoltaic (PV) array have been studied extensively and important observations have been pointed out. Based on these observations, two new maximum power point tracking techniques (MPPTs) are designed: one is specialized for uniform conditions and the other one for non-uniform conditions i.e. partial shading.

For uniform conditions, a novel hybrid MPPT technique has been proposed to optimize the conventional perturb and observe technique. The followings are the highlights of the proposed work: 1) duration of open-circuit voltage measurement has been figured out, 2) relations have been developed, which provide estimations of maximum power point voltage and current, 3) A new duty cycle optimization method is designed, 4) in order to judge the varying weather conditions, the frequency of open-circuit voltage measurement is set and then criteria are formulated with respect to the sampling rate of PV system, and 5) limit criteria are developed to judge the steady weather conditions.

All these features are translated into the control architecture of the proposed technique, which makes it low complex compared to past-proposed MPPTs and yet exhibits better performance. Furthermore, parameters of the proposed technique are discussed with proper formulation such that the researchers of this field can apply the proposed technique with ease. The proposed technique and other techniques are simulated in Matlab/Simulink and performances are verified using the experimental setup consisting of resistive and battery loads. It has been shown through the comparative analysis of experimental and simulation tests that the proposed MPPT has outperformed the other techniques in terms of dynamic and steady state efficiencies.

On the other hand, when PV array is under partial shading condition, the detection of GM is indispensable in order to maximize the PV system energy

production. In this thesis, several critical observations are made out of an extensive study of partial shading using two comprehensive PV models. Most important observations are: PV array exhibits multiple local maxima due to bypass diodes, activation points of bypass diodes are occurred near the multiples of open-circuit voltage of the module and last local maximum always occurs near open-circuit voltage of the array. The working principle of the algorithm is based on these observations. Some of the salient features of the proposed technique are: 1) the method is not complex, yet effective, to track the global maximum and can be implemented by an inexpensive microcontroller, 2) the technique has voltage limit mechanism, which directs the algorithm not to scan the complete power-voltage curve needlessly, and 3) intelligent calibration of voltage steps, which helps the algorithm to search the true global maximum in less voltage perturbations.

All these features ensure the advantage of proposed MPPT over the past-proposed MPPTs in terms of algorithm complexity, accuracy, voltage perturbations and efficiency. To verify the performance of the proposed BD-MPPT, simulations in Matlab/Simulink are performed.

After that, the MPPT for partial shading is further modified in order to enhance the tracking ability of MPPT, i.e. the mission to find the global maximum should be accomplished with less voltage perturbations. And, also it can be integrated with the MPPT designed for uniform condition. The main modification is produced in the global maximum search mechanism of the MPPT, which is based on the prediction of current of the PV array. The tracking ability of modified MPPT has been verified from the analysis of numerous experimental tests. Finally, the two techniques are applied to the experimental data of 86.24 kW building integrated PV plant. Experimental analysis reveals that the operational efficiency of PV plant has improved with the use of modified MPPT.

In addition, a new pulse width modulation (PWM) scheme has been designed in order to adjust the duty cycle (D) of the converter. The working principle is mainly based on the proportional controller. Thus, the scheme is simple as only one parameter (proportional gain) needs to be tuned. At the same time, the mechanism of the scheme is such that it filters out the oscillations inherited by the proportional

controller. Theoretical formulas are provided to set the proportional gain for both resistive as well as battery loads, which reveal that for resistive load the gain is dynamic while it is static for the battery load. Boundary limits of duty cycle are addressed. Also, unlike other direct control schemes, output voltage information is not required for the proposed scheme. Thus making it cost effective. Also, for stable operation of PV systems, two new relations are developed in order to calibrate the value of resistive and battery loads.

# References

- [1] M. Iqbal, M. Azam, M. Naeem, A. Khwaja and A. Anpalagan, "Optimization classification, algorithms and tools for renewable energy: A review," *Renewable and Sustainable Energy Reviews*, vol. 39, pp. 640-654, 2014.
- [2] U.S. Energy Information Administration. *International energy outlook*; 2013.
- [3] IEA, International Energy Agency. *World energy outlook 2009*. Paris: OECD/IEA; 2009.
- [4] B. K. Bose, "Global warming: Energy, environmental pollution, and the impact of power electronics," *IEEE Industrial Electronics Magazine*, vol. 4, no. 1, pp. 6-17, 2010.
- [5] European Renewable Energy Council (2004, May). *Renewable Energy Scenario to 2040* [Online]. Available: [http://www.erec-renewables.org/documents/targets\\_2040/EREC\\_Scenario%202040.pdf](http://www.erec-renewables.org/documents/targets_2040/EREC_Scenario%202040.pdf).
- [6] C. Li, H. Shi, Y. Cao, J. Wang, Y. Kuang, Y. Tan and J. Wei, "Comprehensive review of renewable energy curtailment and avoidance: A specific example in China," *Renewable and Sustainable Energy Reviews*, vol. 41, pp. 1067-1079, 2015.
- [7] IEA. *World energy outlook 2013*. International Energy Agency; 2013. Available at: [http://www.worldenergyoutlook.org/media/weowebiste/2013/WEO2013\\_Ch06\\_Renewables.pdf](http://www.worldenergyoutlook.org/media/weowebiste/2013/WEO2013_Ch06_Renewables.pdf).
- [8] <http://en.wikipedia.org/wiki/Photovoltaics>
- [9] "Market Report 2013 (02)". EPIA-publications. European Photovoltaic Industry Association. March 2014. Archived from the original on 4 April 2014.
- [10] European Photovoltaic Industry Association (2013). "Global Market Outlook for Photovoltaics 2013-2017".
- [11] A. Rockett, "The future of energy – Photovoltaics," *Current Opinion in Solid State and Materials Science*, vol. 14, no. 6, pp. 117-122, 2010.
- [12] [http://en.wikipedia.org/wiki/Solar\\_cell\\_efficiency#cite\\_note-11](http://en.wikipedia.org/wiki/Solar_cell_efficiency#cite_note-11).
- [13] V. Tyagi, N. Rahim, N. Rahim and J. Selvaraj, "Progress in solar PV technology: Research and achievement," *Renewable and Sustainable Energy Reviews*, vol. 20, pp. 443-461, 2013.
- [14] B. Parida, S. Iniyar and R. Goic, "A review of solar photovoltaic technologies," *Renewable and Sustainable Energy Reviews*, vol. 15, no. 3, pp. 1625-1636, 2011.
- [15] J. Etcheverry, "Sustainable Deployment of Photovoltaics: What's Wrong with the Current Policy and Technology Focus?," *The Electricity Journal*, vol. 26, no. 2, pp. 24-31, 2012.

- [16] H. Patel and V. Agarwal, "Maximum Power Point Tracking Scheme for PV Systems Operating Under Partially Shaded Conditions," *IEEE Transactions on Industrial Electronics*, vol. 55, no. 4, pp. 1689-1698, 2008.
- [17] Z. Salam, J. Ahmed and B. Merugu, "The application of soft computing methods for MPPT of PV system: A technological and status review," *Applied Energy*, vol. 107, pp. 135-148, 2013.
- [18] M. Eltawil and Z. Zhao, "Grid-connected photovoltaic power systems: Technical and potential problems—A review," *Renewable and Sustainable Energy Reviews*, vol. 14, no. 1, pp. 112-129, 2010.
- [19] V. Salas, E. Olías, A. Barrado and A. Lázaro, "Review of the maximum power point tracking algorithms for stand-alone photovoltaic systems," *Solar Energy Materials and Solar Cells*, vol. 90, no. 11, pp. 1555-1578, 2006.
- [20] A. Bidram, A. Davoudi and R. Balog, "Control and Circuit Techniques to Mitigate Partial Shading Effects in Photovoltaic Arrays," *IEEE Journal of Photovoltaics*, vol. 2, no. 4, pp. 532-546, 2012.
- [21] E. Koutroulis and F. Blaabjerg, "A New Technique for Tracking the Global Maximum Power Point of PV Arrays Operating Under Partial-Shading Conditions," *IEEE Journal of Photovoltaics*, vol. 2, no. 2, pp. 184-190, 2012.
- [22] G. Petrone, G. Spagnuolo, R. Teodorescu, M. Veerachary and M. Vitelli, "Reliability Issues in Photovoltaic Power Processing Systems," *IEEE Transactions on Industrial Electronics*, vol. 55, no. 7, pp. 2569-2580, 2008.
- [23] T. Eswam and P. Chapman, "Comparison of Photovoltaic Array Maximum Power Point Tracking Techniques," *IEEE Trans. On Energy Conversion*, vol. 22, no. 2, pp. 439-449, 2007.
- [24] A. N. A. Ali, M. H. Saied, M. Z. Mostafa and T. M. Abdel- Moneim, "A Survey of Maximum PPT techniques of PV Systems," in *Proc. IEEE Energytech*, May 2012.
- [25] A. Reza Reisi, M. Hassan Moradi and S. Jamasb, "Classification and comparison of maximum power point tracking techniques for photovoltaic system: A review," *Renewable and Sustainable Energy Reviews*, vol. 19, pp. 433-443, 2013.
- [26] M. Eltawil and Z. Zhao, "MPPT techniques for photovoltaic applications," *Renewable and Sustainable Energy Reviews*, vol. 25, pp. 793-813, 2013.
- [27] K. Ishaque and Z. Salam, "A review of maximum power point tracking techniques of PV system for uniform insolation and partial shading condition," *Renewable and Sustainable Energy Reviews*, vol. 19, pp. 475-488, 2013.
- [28] A. Mellit and S. Kalogirou, "MPPT-based artificial intelligence techniques for photovoltaic systems and its implementation into field programmable gate array chips: Review of current status and future perspectives," *Energy*, vol. 70, pp. 1-21, 2014.
- [29] M. Villalva, J. Gazoli and E. Filho, "Comprehensive Approach to Modeling and Simulation of Photovoltaic Arrays," *IEEE Transactions on Power Electronics*, vol. 24, no. 5, pp. 1198-1208, 2009.

- [30] Kyocera. [Online]. (accessed Oct. 2014) Available <http://www.kyocerasolar.com/assets/001/5195.pdf>
- [31] FVG Ebergly. [Online]. (accessed Oct. 2014) Available [http://www.yeint.fi/files/products/FVG36\\_125\\_ENG.pdf](http://www.yeint.fi/files/products/FVG36_125_ENG.pdf)
- [32] K. Ishaque, Z. Salam and Syafaruddin, "A comprehensive MATLAB Simulink PV system simulator with partial shading capability based on two-diode model," *Solar Energy*, vol. 85, no. 9, pp. 2217-2227, 2011.
- [33] Siemens. [Online]. (accessed Mar. 2015) Available [www.solarquest.com/microsolar/suppliers/siemens/sm55.pdf](http://www.solarquest.com/microsolar/suppliers/siemens/sm55.pdf)
- [34] H. Patel and V. Agarwal, "MATLAB-Based Modeling to Study the Effects of Partial Shading on PV Array Characteristics," *IEEE Trans. On Energy Conversion*, vol. 23, no. 1, pp. 302-310, 2008.
- [35] A. Guechi and M. Chegaar, "Effects of diffuse spectral illumination on microcrystalline solar cells," *J. Electron Devices*, vol. 5, pp. 116-121, 2007.
- [36] W. Shockley, "The theory of p-n junctions in semiconductors and p-n junction transistors," *Bell System Technical Journal*, vol. 28, pp. 435-89, 1949.
- [37] F. Attivissimo, F. Adamo, A. Carullo, A. Lanzolla, F. Spertino and A. Vallan, "On the performance of the double-diode model in estimating the maximum power point for different photovoltaic technologies," *Measurement*, vol. 46, no. 9, pp. 3549-3559, 2013.
- [38] E. Q. B. Macabebe and E. E. van Dyk, "Extraction of device parameters from dark current-voltage characteristics of PV devices," *Physica Status Solidi (c)*, vol. 5, no. 2, pp. 616-619, 2008. [Online]. Available: <http://dx.doi.org/10.1002/pssc.200776834>
- [39] D. Sera, "Real-time Modelling, Diagnostics and Optimised MPPT for Residential PV Systems," Ph.D. dissertation, Faculty of Engineering, Science & Medicine, Aalborg University, Denmark, 2009.
- [40] A. Murtaza, M. Chiaberge, F. Spertino, D. Boero and M. De Giuseppe, "A maximum power point tracking technique based on bypass diode mechanism for PV arrays under partial shading," *Energy and Buildings*, vol. 73, pp. 13-25, 2014.
- [41] K. Ishaque and Z. Salam, "A Deterministic Particle Swarm Optimization Maximum Power Point Tracker for Photovoltaic System under Partial Shading Condition," *IEEE Transactions on Industrial Electronics*, vol. 60, no. 8, pp. 3195-3206, 2013. Confirm reference
- [42] F. Spertino, J.S. Akilimali, "Are manufacturing I-V mismatch and reverse currents key factors in large photovoltaic arrays?," *IEEE Transactions on Industrial Electronics*, vol. 56, no. 11, pp. 4520-4531, 2009.
- [43] R. Mastromauro, M. Liserre and A. Dell'Aquila, "Control Issues in Single-Stage Photovoltaic Systems: MPPT, Current and Voltage Control," *IEEE Transactions Ind. Inf.*, vol. 8, no. 2, pp. 241-254, 2012.
- [44] E. Molenbroek, D.W. Waddington, K.A. Emery, "Hot spot susceptibility and testing of PV modules," *22nd IEEE Photovoltaic Specialists Conference*, vol. 1, pp. 547-552, 1991.

- [45] A. Murtaza, M. Chiaberge, M. Giuseppe and D. Boero, "A duty cycle optimization based hybrid maximum power point tracking technique for photovoltaic systems," *International Journal of Electrical Power & Energy Systems*, vol. 59, pp. 141-154, 2014.
- [46] S. Silvestre, A. Boronat and A. Chouder, "Study of bypass diodes configuration on PV modules," *Applied Energy*, vol. 86, no. 9, pp. 1632-1640, 2009.
- [47] P. Peter and Vivek Agarwal, "On the Input Resistance of a Reconfigurable Switched Capacitor DC-DC Converter-Based Maximum Power Point Tracker of a Photovoltaic Source," *IEEE Transactions on Power Electronics*, vol. 27, no. 12, pp. 4880-4893, 2012.
- [48] J. Soon and K. Low, "Photovoltaic Model Identification Using Particle Swarm Optimization With Inverse Barrier Constraint," *IEEE Transactions on Power Electronics*, vol. 27, no. 9, pp. 3975-3983, 2012.
- [49] G. de-Cesare, D. Caputo and A. Nascetti, "Maximum power point tracker for portable photovoltaic systems with resistive-like load," *Solar Energy*, vol. 80, pp. 982-988, 2006.
- [50] S. Shao, M. Yin, L. Xu and Y. Wang, "T-S Fuzzy Control for Maximum Power Point Tracking of Solar Power Generation Systems," *AMM*, vol. 84-85, pp. 120-124, 2011.
- [51] M. Miyatake, M. Veerachary, F. Toriumo, N. Fuhi and H. Ko, "Maximum power point tracking of multiple photovoltaic arrays: A PSO approach," *IEEE Transactions on Aerospace and Electronic Systems*, vol. 47, no. 1, pp. 367-380, Jan. 2011.
- [52] J. J. Soon and K-S. Low, "Photovoltaic Model Identification Using Particle Swarm Optimization With Inverse Barrier Constraint," *IEEE Transactions on Power Electronics*, vol. 27, no. 9, pp. 3975-3983, Sept. 2012.
- [53] C-S. Chiu, "T-S fuzzy maximum power point tracking control of solar power generation systems," *IEEE Transactions on Energy Conversion*, vol. 25, no. 4, pp. 1123-1132, Dec. 2010.
- [54] T. L. Kottas, Y. S. Boutalis and A. D. Karlis, "New maximum power point tracker for PV arrays using fuzzy controller in close cooperation with fuzzy cognitive networks," *IEEE Transactions on Energy Conversion*, vol. 21, no. 3, pp. 793-1132, Sept. 2006.
- [55] K. Ishaque, Z. Salam and G. Lauss, "The performance of perturb and observe and incremental conductance maximum power point tracking method under dynamic weather conditions," *Applied Energy*, vol. 119, pp. 228-236, 2014.
- [56] D. P. Hohm and M. E. Ropp, "Comparative study of maximum power point tracking algorithms," *Progress in Photovoltaics: Research and Applications*, vol. 11, pp. 47-62, 2003.
- [57] E. Bianconi, J. Calvente, R. Giral, E. Mamarelis, G. Petrone, C. A. Ramos-Paja, G. Spagnuolo, M. Vitelli, "Perturb and observe MPPT algorithm with a current controller based on the sliding mode," *Electrical Power and Energy Systems*, vol. 44, pp. 346-356, 2013.

- [58] AMZ Alabedin, EF El-Saadany, MMA Salama , “Maximum power point tracking for photovoltaic systems using fuzzy logic and artificial neural networks,” IEEE Power Energy Soc Gen Meet, 2011–9.
- [59] A. K. Abdelsalam, A. M. Massoud, S. Ahmed and P. N. Enjeti, “High-performance adaptive perturb and observe MPPT technique for photovoltaic-based microgrids,” IEEE Transactions on Power Electronics, vol. 26, no. 4, pp. 1010–1021, Apr. 2011.
- [60] J. S. C. M. Raj and A. E. Jeyakumar, “A novel maximum power point tracking technique for photovoltaic module based on power plane analysis of I–V characteristics,” IEEE Transactions on Industrial Electronics, vol. 61, no. 9, pp. 4734–4745, Sept. 2014.
- [61] F. Zhang, K. Thanapalan, A. Procter, S. Carr and J. Maddy, “Adaptive hybrid maximum power point tracking method for a photovoltaic system,” IEEE Transactions on Energy Conversion, vol. 28, no. 2, pp. 353–360, Jun. 2013.
- [62] T. Tafticht, K. Agbossou, M.L. Doumbia and A. Che’riti, “An improved maximum power point tracking method for photovoltaic systems,” Renewable Energy, vol. 33, pp. 1508–1516, 2007.
- [63] M. H. Moradi and A. R. Reisi, “A hybrid maximum power point tracking method for photovoltaic systems,” Solar Energy, vol. 85, pp. 2965–2976, 2011.
- [64] F. Spertino, J. Sumaili, H. Andrei and G. Chicco, “PV module parameter characterization from the transient charge of an external capacitor,” IEEE Journal of Photovoltaics, vol. 3, no. 4, pp. 1325–1333, Oct. 2013.
- [65] J. Qi, Y. Zhang and Y. Chen, “Modeling and maximum power point tracking (MPPT) method for PV array under partial shade conditions,” Renewable Energy, vol. 66, pp. 337–345, 2014.
- [66] A. M. Latham, R. Pilawa-Podgurski, K. M. Odame and C. R. Sullivan, “Analysis and optimization of maximum power point tracking algorithms in the presence of noise,” IEEE Transactions on Power Electronics, vol. 28, no. 7, pp. 3479–3494, Jul. 2013.
- [67] N. Femia, G. Petrone, G. Spagnuolo and M. Vitelli, “Optimization of perturb and observe maximum power point tracking method,” IEEE Transactions on Power Electronics, vol. 20, no. 4, pp. 963–973, Jul. 2005.
- [68] S. Daraban, D. Petreus and C. Morel, “A novel MPPT (maximum power point tracking) algorithm based on a modified genetic algorithm specialized on tracking the global maximum power point in photovoltaic systems affected by partial shading,” Energy, vol. 74, pp. 374–388, 2014.
- [69] S. Vergura, G. Acciani, V. Amoroso, G. E. Patrono, and F. Vacca, “Design and application for PV generation system using a soft-switching boost converter with SARC,” IEEE Transactions on Industrial Electronics, vol. 57, no. 2, pp. 515–522, Feb. 2010.
- [70] A. Maki and S. Valkealahti, “Power losses in long string and parallel-connected short strings of series-connected silicon-based photovoltaic modules due to partial shading conditions,” IEEE Transactions on Energy Conversion, vol. 27, no. 1, pp. 173–183, Mar. 2012.

- [71] E. V. Paraskevadaki and S. A. Papathanassiou, "Evaluation of MPP voltage and power of mc-Si PV modules in partial shading conditions," *IEEE Transactions on Energy Conversion*, vol. 26, no. 3, pp. 923-932, Sept. 2011.
- [72] K. Ding, X. G. Bian, H. H. Liu, and T. Peng, "A MATLAB-Simulink-based PV module model and its application under conditions of nonuniform irradiance," *IEEE Transactions on Energy Conversion*, vol. 27, no. 4, pp. 864-872, Dec. 2012.
- [73] Y-H. Ji, D-Y. Jung, J-G. Kim, J-H. Kim, T-W. Lee and C-Y. Won, "A real maximum power point tracking method for mismatching compensation in PV array under partially shaded conditions," *IEEE Transactions on Power Electronics*, vol. 26, no. 4, pp. 1001-1009, Apr. 2011.
- [74] A. Kouchaki, H. Iman-Eini and B. Asaei, "A new maximum power point tracking strategy for PV arrays under uniform and non-uniform insolation conditions," *Solar Energy*, vol. 91, pp. 221-232, 2013.
- [75] S. Subiyanto, A. Mohamed and M.A. Hannan, "Intelligent maximum power point tracking for PV system using Hopfield neural network optimized fuzzy logic controller," *Energy and Buildings*, vol. 51, pp. 29-38, 2012.
- [76] M. F. N. Tajuddin, S. M. Ayob, Z. Salam and M. S. Saad, "Evolutionary based maximum power point tracking technique using differential evolution algorithm," *Energy and Buildings*, vol. 67, pp. 245-252, 2013.
- [77] L. L. Jiang, D. L. Maskell and J. C. Patra, "A novel ant colony optimization-based maximum power point tracking for photovoltaic systems under partially shaded conditions," *Energy and Buildings*, vol. 58, pp. 227-236, 2013.
- [78] M. Drif, P. J. P´erez, J. Aguilera, and J. D. Aguilar, "A new estimation method of irradiance on a partially shaded PV generator in grid-connected photovoltaic systems," *Renewable Energy*, vol. 33, pp. 2048–2056, Sep. 2008.
- [79] H. Andrei, V. Dogaru-Ulieru, G. Chicco, C. Cepisca and F. Spertino, "Photovoltaic applications," *Journal of Materials Processing Technology*, vol. 181, pp. 267-273, 2007.
- [80] F. Salem, M. S. A-Moteleb, and H. T. Dorrah, "An enhanced fuzzy-PI controller applied to the MPPT problem," *J. Sci. Eng.*, vol. 8, no. 2, pp. 147–153, 2005.
- [81] H. Patel and V. Agarwal, "PV based distributed generation with compensation feature under unbalanced and non-linear load conditions for a 3-f, 4 wire system," in *Proc. IEEE Int. Conf. Ind. Technol.*, Mumbai, India, Dec. 2006, pp. 322–327.